

Accepted to The Astrophysical Journal on June 9, 1998

AN OPTICAL/NEAR-INFRARED STUDY OF RADIO-LOUD QUASAR ENVIRONMENTS II. IMAGING RESULTS

Patrick B. Hall^{1 2}

Steward Observatory, The University of Arizona, Tucson, Arizona 85721
Electronic Mail: hall@astro.utoronto.ca

Richard F. Green

National Optical Astronomy Observatories, Tucson, Arizona 85726-6732
Electronic Mail: rgreen@noao.edu

ABSTRACT

We have previously reported a significant excess of $K_{\geq 19}$ galaxies in the fields of a sample of 31 $z=1-2$ quasars (Hall, Green & Cohen 1998). Here we examine the properties of this excess galaxy population using optical and near-IR imaging.

The excess occurs on two spatial scales. One component lies at $\theta < 40''$ from the quasars and is significant compared to the galaxy surface density at $\theta > 40''$ in the same fields. The other component appears roughly uniform to $\theta \sim 100''$ and is significant compared to the galaxy surface density seen in random-field surveys in the literature.

The $r-K$ color distributions of the excess galaxy populations are indistinguishable, and are significantly redder than the color distribution of the field population. The excess galaxy population is consistent with being predominantly early-type galaxies at the quasar redshifts, while there is no evidence that it is associated with intervening Mg II absorption systems. The average excess within $0.5h_{75}^{-1}$ Mpc ($\sim 65''$) of the quasars corresponds to Abell richness class ~ 0 compared to the galaxy surface density at $>0.5h_{75}^{-1}$ Mpc from the quasars, and to Abell richness class ~ 1.5 compared to that from the literature. We estimate $-0.65_{-0.55}^{+0.41}$ magnitudes of evolution in M_K^* to $\bar{z}=1.67$ by assuming the excess galaxies are at the quasar redshifts.

We discuss the spectral energy distributions (SEDs) of galaxies in fields with data in several passbands. Most candidate quasar-associated galaxies are consistent with being 2-3 Gyr old early-types at the quasar redshifts of $z \sim 1.5$. However, some objects have SEDs consistent with being 4-5 Gyr old at $z \sim 1.5$, and a number of others are

¹Visiting Student, Kitt Peak National Observatory, National Optical Astronomy Observatories, operated by AURA Inc., under contract with the National Science Foundation.

²Current address: Department of Astronomy, University of Toronto, 60 St. George Street, Toronto, Ontario, Canada M5S 3H8

consistent with ~ 2 Gyr old but dust-reddened galaxies at the quasar redshifts. These potentially different galaxy types suggest there may be considerable dispersion in the properties of early-type cluster galaxies at $z \sim 1.5$. There is also a population of galaxies whose SEDs are best modelled by background galaxies at $z \gtrsim 2.5$.

Subject headings: Surveys — Quasars: General — Galaxies: General, Clusters of Galaxies

1. Introduction

With continuing advances in instrumentation now enabling detailed studies of very faint and distant galaxies, it is useful to seek efficient methods to find galaxies and clusters at $z > 1$. One such possible method is to look for galaxies associated with quasars, specifically the radio-loud quasars (RLQs) which comprise $\lesssim 10\%$ of the quasar population.

Radio-quiet quasars (RQQs) are rarely found in clusters at any redshift, but $\sim 35\%$ of intrinsically luminous ($M_B < -25$) RLQs are located in clusters of Abell richness class 0–1 (and occasionally 2) at $z = 0.5–0.7$ (Yee & Green 1987). These quasar host clusters typically have anomalously low X-ray luminosities L_X (Hall *et al.* 1995; Hall, Ellingson & Green 1997) and velocity dispersions σ_v for their richnesses, and thus may be younger and less virialized than optically-selected clusters (Ellingson, Green & Yee 1991; hereafter EGY91). In addition, RLQ environments are known to evolve rapidly and differentially. At $z < 0.5$ only low luminosity RLQs are seen in richness 1 clusters, whereas at $z = 0.5–0.7$ both high and low luminosity RLQs can be found in such environments. A similar effect is seen for FR II radio galaxies (Hill & Lilly 1991). EGY91 model this evolution by postulating that galaxy interactions (more frequent in young, low- σ_v clusters) are largely responsible for creating and fueling RLQs, which then fade as the interaction rate decreases in their evolving, virializing host clusters. Yee & Ellingson (1993) suggested that if the cluster formation rate dropped at $z \sim 0.7$, most quasars we see in rich clusters at $z < 0.7$ would be old ones fading on the host cluster’s dynamical timescale, and that luminous RLQs might be found in rich clusters at $z > 0.7$. The outstanding feature of quasar evolution is the sharp peak in space density and/or luminosity at $z \sim 2–3$ (Shaver *et al.* 1996), but little work has previously been done on quasar environments at $z > 0.7$.

Some RLQs show possible additional evidence for being located in rich environments, in the form of an excess number of “associated” C IV (Foltz *et al.* 1988) or Mg II (Aldcroft, Bechtold & Elvis 1994) absorption systems within ± 5000 km s $^{-1}$ of the quasar redshift. There is a tendency for associated absorption to be preferentially found in steep spectrum sources. Anderson *et al.* (1987) quote a 2σ preference for associated C IV in the unpublished Radio-Loud Survey of Foltz *et al.* This can be seen in Fig. 3 of Foltz *et al.* (1988): 16 of 22 RLQs with strong associated C IV absorption have steep radio spectra, whereas only ~ 10 would be expected. As discussed in

Aldcroft, Bechtold & Elvis (1994), this dependence is also suggested by the studies of Foltz *et al.* (1986) and Sargent, Boksenberg & Steidel (1988). Associated absorption systems may arise in gas expelled at high velocity from the quasars or in galaxies in clusters at or near the quasar redshifts. In the last few years detailed spectroscopy has shown that some associated C IV systems are almost certainly intrinsic to the quasars, as discussed in the introduction to Paper 1 (Hall, Green & Cohen 1998). However, it remains possible that a substantial fraction of such quasars reside in clusters which produce associated absorption. Spectroscopic and imaging approaches are complementary ways to investigate this question.

In 1994 we embarked upon a project to study the environments of RLQs to $z=2.0$, to study any correlations between RLQ environment and quasar properties such as associated absorption, and to study any examples of high-redshift galaxies and/or clusters found in RLQ fields. Paper 1 (Hall, Green & Cohen 1998) describes our sample and observations as well as our data reduction and cataloguing techniques. We observed $\lesssim 3' \times 3'$ fields around 33 RLQs with $z=1-2$ and two control fields with typical 3σ limits of $r=25.5$, $K_s=20.5$ for $z<1.4$, and $K_s=21$ for $z>1.4$. An unusual aspect of our data reduction procedure is the creation of images with constant RMS noise from mosaiced images with exposure times that vary from pixel to pixel. A 3σ detection thus represents a brighter galaxy at the edge of an image than in the center, but as long as the exposure time is everywhere $\geq 36\%$ of the maximum, the average 5σ magnitude limit will be greater than the 3σ detection limit across the entire field. Object detection was done on RMS-weighted sums of the r , K_s , and J data (where available). Photometry was done in all filters using the detection aperture from the summed image. We use FOCAS total magnitudes and colors determined from FOCAS isophotal magnitudes. The useful area surveyed consists of 221 arcmin² of RLQ fields and 19 arcmin² of control fields. Our control field galaxy counts (and color distribution; see Appendix A) are consistent with the literature average, but the statistical uncertainties are unacceptably large for our purposes, so we also assembled a comprehensive set of random-field galaxy surveys from the literature for comparison. One complication arises from comparison with this literature sample: our 1994 and 1995 photometric solutions produce a K -band galaxy number-magnitude relation $N(m)$ slightly higher than the literature at bright magnitudes. Given the possible systematic differences between the various K -band surveys, we conduct some of our analyses using a *conservative* magnitude scale (defined so that our number counts exactly match the literature around $K=17$) as well as our original *liberal* magnitude scale. Both scales use UKIRT K magnitudes; the only differences between them are systematic offsets: on the conservative scale the 1994 magnitudes (mostly $z>1.4$ objects) are 0^m06 fainter than the liberal scale, and the 1995 magnitudes (mostly $z<1.4$) are 0^m12 fainter, for an average difference of $\sim 0^m08$ given the numbers of galaxies in each subsample. As seen in Figure 1, even under our conservative magnitude scaling the galaxy counts at $K_s \gtrsim 19$ in 31 RLQ fields with good data are higher than those of field surveys; i.e., *there is an excess of galaxies in our combined RLQ fields.*

This paper analyzes the excess galaxy population found in Paper 1. In §2 we show that there is an excess of galaxies spatially concentrated around the quasars themselves (see Figure 2). In §3

we show that the excess does not have the same $r-K_s$ color distribution as the field population described in Appendix A (see Figure 11). In §4 we quantify the strength of the clustering under the assumption it is associated with the quasars and look for correlations between clustering strength and various quasar properties. In §5 we estimate the amount of luminosity evolution bright galaxies have undergone in the K -band since $z=1-2$. In §7 we compare the spectral energy distributions of galaxies in several fields with the predictions of various galaxy spectral evolution models. We summarize our major results in §8. Some additional details are found in Hall (1998).

2. Are the Excess Galaxies Associated with the Quasars?

We consider whether the excess galaxies are plausibly physically associated with the quasars by examining the projected radial distribution of galaxies around the quasars and the galaxies' distribution in color-magnitude space. An alternate possibility is that they are intervening galaxies present because they trace large-scale matter fluctuations which weakly lens the quasars, resulting in quasars from radio catalogs with bright flux limits preferentially having galaxy excesses around them (“magnification bias”; see Benítez, Martínez-González & Martín-Mirones 1997 and references therein). We observe 134 galaxies in the magnitude range $K_{UKIRT}=14.5-17$ under our conservative magnitude scaling, and 150 under our liberal magnitude scaling. The average literature counts compiled in §4 of Paper 1 predict 120.3 ± 22.6 galaxies in our survey area, where the uncertainty is the RMS scatter among the different surveys in the literature. Thus the excess of bright $K_{UKIRT} < 17$ galaxies in our fields is not statistically significant, and magnification bias is unlikely to be a significant effect in our sample.

2.1. Projected Radial Distributions of Galaxies Relative to Quasars

If the faint excess galaxies in our fields are physically associated with the quasars, they are likely to lie preferentially near the quasars on the sky. To test this we examine the projected radial distribution of galaxies around the quasars, despite its insensitivity to clusters or groups at the quasar redshift but not centered on the quasars. A matched filter (Postman *et al.* 1996) or cell count (Lidman & Peterson 1996) technique could be used to search for off-center clusters, but would be difficult given the small size of our fields. However, the galaxy excess over each entire field should still reflect the presence of off-center clusters.

For this analysis we excluded the fields of Q 0736–063 (uncertain stellar contamination) and Q 1508–055 (no r data). We took all galaxies detected at $\geq 3\sigma$ down to the average 5σ K magnitude limit in the 31 other fields, above which essentially no spurious detections are expected (see §3.6.7 of Paper 1). We binned the galaxies in $10''$ annuli centered on the quasar and divided by the area imaged within each annulus. No correction was made for loss of objects due to crowding or incompleteness or for stars fainter than our star-galaxy classification limits, and we do

not count the quasar host galaxy. None of these effects should significantly bias the radial galaxy distribution. The results (Figure 2) show a clear excess of galaxies within $40''$ of the quasars. The data at $\theta < 40''$ deviates from the level determined from the $\theta > 40''$ data at the 99.999% significance level (4.5σ , assuming a gaussian probability distribution).

We use the reduced chi-squared χ_ν^2 to quantify the deviation from a uniform radial distribution. Here ν is the number of radial bins used minus the number of parameters determined from the data. We use χ_ν^2 both for the deviation from the literature across the entire field and for the deviation of the $\theta < 40''$ data from the $\theta > 40''$ data. Since the χ_ν^2 test requires binning and does not distinguish over- and under-densities in individual bins, we also use the Kolmogorov-Smirnov test, which requires no binning but is less sensitive to differences in the tails of the distributions (small or large radii) than in the middle.

To investigate the magnitudes of the galaxies producing the observed excess at $\theta < 40''$, we take all galaxies with $K_s < 17$ and repeat our analysis. The results are consistent with a uniform distribution. This is a strong indication that at least some of the faint excess galaxies in these fields are associated with the quasars, since both bright (i.e., $z < 1$) and faint galaxies should be involved if intervening lensing galaxies caused the excess at $\theta < 40''$.

2.1.1. Dependence on Quasar Redshifts

To search for any dependence of the galaxy excess on the quasar redshifts, we split the quasar sample into $z < 1.4$ and $z > 1.4$ subsamples. This is a natural division since the two subsamples were observed almost entirely in different observing runs, and so any systematic magnitude scale offsets will not affect comparisons within them. Also, the $z > 1.4$ imaging reaches deeper than the $z < 1.4$ imaging in an absolute sense as well as relative to the estimated brightest cluster galaxy magnitude at the average subsample z . Repeating our analysis for low- and high-redshift subsamples with equal numbers of quasars does not change our results in either a qualitative or a significant quantitative sense. Figure 3 shows the ensemble radial profile for the high-redshift subsample, which deviates from the uniform level of the $\theta > 40''$ bins at 99.83% (3.15σ) significance (from the K-S test). The data at $\theta < 40''$ deviates from the $\theta > 40''$ prediction at the 99.99% (3.9σ) level. The amplitude and spatial profile of the central excess are both consistent with it being composed of galaxy clusters at the quasar redshifts. For the $z < 1.4$ RLQ fields, we plot only objects brighter than 0^m45 above the average 5σ K limit, equivalent to 7.5σ detections, to ensure uniform detection sensitivity at all radii in spite of different exposure times. Figure 4 shows a possible overall excess within $30''$, but no excess in the innermost $10''$. The overall dataset deviates from the $\theta > 40''$ prediction at only 65% significance (1σ) and the $\theta < 40''$ data at only the 97% (2.2σ) level, due to the large uncertainties (our $z < 1.4$ field data is shallower than our $z > 1.4$ field data). The $\theta < 10''$ deficit persists even in the complete catalog of 3σ detections in either r or K_s and is not caused by incompleteness due to seeing or inappropriate dithering. This deficit may indicate that the $z < 1.4$ quasars are not centered in any putative host clusters, but excluding the innermost

point does not raise the significance of the $\theta < 40''$ excess above 3σ . If the $\theta < 40''$ excess is real, the $\theta < 10''$ deficit argues against it being due to foreground lensing galaxies.

2.1.2. Large-Scale Excess

The excess galaxies in the central $\sim 40''$ radius region cannot explain the entire excess observed in our fields. In Figure 5 we plot the radial distribution of galaxies to a fixed limit of $K_{UKIRT}=19.5$ along with the surface density and $\pm 1\sigma$ RMS dispersion derived from the average published literature counts. Despite the large uncertainties, there are apparently two components to the excess galaxies: the central component ($\theta < 40''$) and a large-scale component extending to $\theta \sim 100''$. (At $z \sim 1.5$ in our $H_0=75$, $q_0=0.1$ cosmology, $40''$ is $\sim 0.3h_{75}^{-1}$ Mpc and $100''$ is $\sim 0.75h_{75}^{-1}$ Mpc.) Could this large-scale component be spurious? The RMS uncertainties on the combined literature counts are in good agreement with galaxy clustering predictions based on single surveys (Carlberg *et al.* 1997; Roche, Eales & Hippelein 1997), so the range shown for the literature should be accurate. We do not expect many spurious objects above the 5σ limits in our fields. We have neglected contamination by stars fainter than our star-galaxy classification limits, but also incompleteness corrections to our fields (though not to the literature data). If we include both effects, the galaxy surface density is essentially unchanged to $K_{UKIRT}=20$ and actually increases (by $\lesssim 3\%$) to $K_{UKIRT}=20.5$.

A simple check of the need for a large-scale excess can be made: from Figure 2, the central excess at $\theta < 40''$ above the surface density defined by the $\theta > 40''$ points is only $\sim 10\%$ of the total counts, or 0.04 dex, but Figure 1 shows that our excess counts are ~ 0.1 dex (25%) above the literature average at $19 < K_{UKIRT} < 21.5$. Thus a large-scale excess of amplitude roughly equal to the central excess must exist in our fields. Supporting evidence for the reality of the large-scale excess can be found in its $r-K_s$ color distribution (Figure 14), which is indistinguishable from that of the excess at $\theta < 40''$.

2.1.3. Ubiquity of the Excess Galaxies

We consider various subsamples of our data to see how common the excess galaxies are. We plot the radial distribution of galaxies in our $z > 1.4$ fields to various limits in Figure 6. Using the average surface density from the $\theta > 40''$ data, the $\theta < 40''$ excess has significance 99.7% (3σ) at $K < 20.5$, and $\leq 85\%$ ($\leq 1\sigma$) at $K < 20$ or brighter. Using the average literature surface density and RMS, the overall excess (central and large-scale) has significance 99.9% (3.3σ) at $K < 20.5$ or $K < 20$ and $< 95\%$ (2σ) at $K < 19.5$ or $K < 19$. Using our conservative magnitude scale effectively moves the literature surface density upward slightly. The overall excess then has significance of only 96–97% (2 – 2.2σ) at $K < 20.5$ or $K < 20$. Thus for our $z > 1.4$ fields alone, the central excess is only significant if the magnitude limit reaches $K=20.5$, while the large-scale excess is only

significant if the magnitude limit is $K=20$ or fainter, and then only under our liberal magnitude scale. Due to shallower magnitude limits and fewer fields, the uncertainties are larger at $z<1.4$ (Figure 7). The overall excess compared to the average surface density from the literature is only significant at the 95% (2σ) level at best, and even less under our conservative magnitude scaling. We have confidence in the reality of this large-scale excess despite these low formal significances, since the limiting factor in determining the significance is the intrinsically large field-to-field RMS of K -band galaxy counts.

The central excess may be produced by only a few of the fields, but the large-scale excess is not. If we exclude the 5 (out of 20) $z>1.4$ fields with highest χ^2 , the central excess drops below 3σ significance. Thus it may be produced by as few as $\sim 25\%$ of the fields (a *very* uncertain fraction). However, if we take the 15 $z>1.4$ fields which reach $K=20$ and remove the 5 fields with highest χ^2 , the resulting overall excess is still significant at the 99.7% (3σ) level, as measured by both the χ^2 and K-S tests. Thus the large-scale galaxy excess is not produced solely by the same fields which may contribute most of the central galaxy excess. At least $\sim 50\%$ of our RLQ fields contribute to the large-scale galaxy excess. Both fractions may be higher since removing fields will reduce the S/N and significance (to $<3\sigma$) even when all fields contribute to the large-scale excess.

Only three of our fields might have a large-scale excess produced by very low redshift galaxy associations listed in NED³ within $18'$: Q 1018+348, $7'4$ from Abell 982 (no published redshift); Q 1221+113, $1'7$ from the center of the Virgo cluster and $7'4$ from NGC 4352, and Q 2230+114, $5'5$ from NGC 7305. Excluding them does not significantly reduce the χ^2_{ν} of any fit. Another remote possibility is that faint galaxies associated with the supergalactic plane (De Vaucouleurs 1975) might affect our counts. Using NED, we found the average absolute supergalactic latitudes to be $31\pm 17^\circ$ for our $z=1-1.4$ RLQ subsample, $27\pm 16^\circ$ for our $z=1.4-2$ RLQ subsample, and $23\pm 14^\circ$ for published random-field K -band surveys. Thus even if faint galaxy counts do correlate with supergalactic latitude, there should be no systematic offset between our counts and those of the published literature data due to such an effect.

2.2. Correlations with Quasar Properties

Finally, we examine the dependence of the central excess on various quasar properties using the χ^2 test. Ordering our sample on absolute V magnitude and splitting it in half, we find a 4σ $\theta<40''$ excess for the more luminous RLQs ($M_V=-27.21\pm 0.61$) but only a 2σ excess for the fainter RLQs ($M_V=-25.31\pm 0.77$). However, these subsamples have average redshifts $\bar{z}=1.64\pm 0.27$ and 1.32 ± 0.28 respectively. The central excess is more significant in our $z>1.4$ subsample than in our $z<1.4$ subsample. Thus we cannot say whether the primary dependence is on M_V or redshift. In

³The NASA/IPAC Extragalactic Database (NED) is operated by the Jet Propulsion Laboratory, California Institute of Technology, under contract to NASA.

fact, the apparent redshift dependence may be due to the fact that our $z > 1.4$ data reaches an average of $2^m 4$ below K_{BCG} (K_{BCG} is the estimated brightest cluster galaxy magnitude at the quasar redshifts), as opposed to $2^m 1$ below K_{BCG} for our $z < 1.4$ data (see §4.2). This is in turn because our 1995 IRIM data (mostly $z < 1.4$ objects) has higher backgrounds and poorer seeing than our 1994 IRIM data (mostly $z > 1.4$ objects).

Similarly splitting the sample in half at radio power $\log P_{rad} = 27.5$ W/Hz, we find a $> 4\sigma$ $\theta < 40''$ excess for more powerful RLQs ($\log P_{rad} = 27.79 \pm 0.21$) but only 2σ for less powerful ones ($\log P_{rad} = 27.14 \pm 0.37$). The average redshifts of these subsamples are 1.46 ± 0.32 and 1.49 ± 0.32 respectively, and the average M_V are -26.20 ± 1.40 and -26.26 ± 0.95 , so this does seem to be a dependence on radio power.

If we compare the 11 flat-radio-spectrum and 19 steep-radio-spectrum objects, we find a 3.6σ $\theta < 40''$ excess around the steep-spectrum objects but only a 1.65σ excess around the flat-spectrum ones. These two subsamples have very well-matched redshift, M_{abs} , and P_{rad} distributions, so again the dependence seems to be on radio spectrum. This is supported by the results of splitting the sample between sources with and without strong radio lobes (types FR II or T and types C or CE, respectively, in Table 1 of Paper 1), subsamples which are 84% and 25% steep-spectrum objects respectively. For strong-lobed sources we see a 3.4σ $\theta < 40''$ excess, while for weak-lobed sources the excess is only 2.6σ .

Splitting our sample according to the quasars' associated absorption properties, we find a 2.8σ $\theta < 40''$ excess in 13 objects with associated absorption and a 2.4σ excess in 9 objects with no associated absorption. These subsamples are slightly mismatched in M_V , but well matched in z and P_{rad} . Detecting excesses around steep-spectrum RLQs but not ones with associated absorption may be surprising in light of the $\gtrsim 2\sigma$ tendency for steep-spectrum RLQs to preferentially show associated absorption (see the introduction to Paper 1). However, this tendency is not strong enough and our subsamples are not large enough to show a significant contradiction.

2.3. Summary and Discussion: Radial Profiles

We see an excess of galaxies at $\theta < 40''$ from these 31 RLQs compared to the $\theta > 40''$ background level. This central excess is significant at the $\sim 99.995\%$ ($\sim 4\sigma$) level and consists of $K > 17$ galaxies. It is seen at $3-4\sigma$ significance in the $z > 1.4$ fields, but only at $\sim 2\sigma$ significance in the $z < 1.4$ fields which are shallower and fewer in number. The central excess at $z > 1.4$ may be produced by as few as 5 of the 20 fields, but it is not due to one or two extreme outliers. There is an additional large-scale galaxy excess extending to $\theta \sim 100''$ detectable in our $z > 1.4$ fields with 3.3σ significance at $K < 20$ or $K < 20.5$. It may also be present in our $z < 1.4$ fields, but the larger uncertainties there preclude a detection above 2σ . We consider various possible errors and conclude that the large-scale excess is real at the given significance levels, and that it is not produced solely by the same fields which may contribute most of the central galaxy excess. The $\theta < 40''$ excess does

not depend on the presence of associated absorption, but seems to be stronger (4σ vs. 2σ) for the more radio-powerful RLQs, and may be stronger (3.6σ vs. 1.65σ) for steep-radio-spectrum ($\alpha_r \geq 0.5$) RLQs than for flat-spectrum ones.

Could the excess galaxies be associated with intervening Mg II absorption-line systems? This is difficult to quantify this using radial profiles due to the variation in limiting magnitude between fields and the low formal significances of the excesses at all but the faintest magnitudes. However, we show in §4.3 that the 8 $z > 1.4$ RLQs with known intervening absorption and the 8 $z > 1.4$ RLQs without it show no differences in their inferred richnesses. Thus there is no evidence that galaxies associated with intervening Mg II systems contribute significantly to the observed galaxy excess.

The large-scale (to $\theta \sim 100''$) excess can plausibly be located at the quasar redshifts. At $z = 1.4 - 2.0$, a $200''$ diameter circle corresponds to $\sim 1.5h_{75}^{-1}$ Mpc diameter, which is not an implausibly large scale, especially if it is connected with the $\theta < 40''$ ($0.6h_{75}^{-1}$ Mpc diameter) excess which might be e.g. a cluster core or group embedded in a larger overdensity. From the PLE model redshift distribution of Roche, Eales & Hippelein (1997), we estimate that $\sim 1.5 \pm 0.5\%$ of field galaxies to $K = 20$ lie within $\delta z = 0.05$ of $z = 1.70$. This redshift bin size is large but similar to those in which overdensities have been spectroscopically confirmed at high z (Dickinson 1996b; Steidel *et al.* 1998a). Our observed galaxy surface density to $K = 20$ is 1.23 ± 0.14 times the literature (Figure 6). Thus if all this excess was at the quasar redshifts, it would constitute a typical galaxy number overdensity of $\sim 14 \pm 10$ compared to the model redshift distribution. This overdensity is again plausible: virialized clusters are overdense by similar factors on similar scales, the RMS galaxy fluctuation on $8h^{-1}$ Mpc scales is $\sigma_8 \simeq 1$ (Lin *et al.* 1996), and superclusters have overdensities $\sim 5 - 40$ on $\sim 30h^{-1}$ Mpc scales (Small *et al.* 1998). The candidate large-scale structures in these fields are not unprecedented; they would be similar to the galaxy overdensities of ~ 10 spectroscopically confirmed by Deltorn *et al.* (1996; 1997) and Dickinson (1996b) at and/or near the redshifts of three $z \sim 1$ radio galaxies on very similar spatial scales. In particular, the overdensity near 3C 324 (Dickinson 1996b) is composed of two clumps or sheets of galaxies separated by $\sim 7500 \text{ km s}^{-1}$ in their rest frame, evidence for the existence of large-scale structures around at least some $z > 1$ radio-loud AGN. Similarly, the $8'$ -separation $z = 0.6$ quasar pair 3C 345 and Q 1641+3998 may be embedded in a large-scale galaxy structure (Ellingson & Yee 1994).

3. Color-Magnitude Diagrams

Color-magnitude diagrams (hereafter CMDs and denoted as magnitude/color, e.g. $K_s/r - K_s$) can provide useful information on the excess galaxies in our fields. Since field galaxies contaminate CMDs at all magnitudes and colors, comparison of quasar-field and control-field CMDs must be made. We discuss the literature control field datasets we use in Appendix A.

To reduce the uncertainties on the colors, we calculate them using FOCAS isophotal magnitudes. We use the same aperture in all filters, namely the isophotal aperture from the

coadded $r+K_s$ or $r+J+K_s$ detection image for the field. This also allows for more accurate color limits, since measuring colors through smaller apertures allows very faint objects to be detections instead of 3σ upper limits. Comparison of isophotal- and total-aperture colors showed no systematics and a scatter consistent with photometric uncertainties.

Figure 8 shows the $K_s/r-K_s$ CMD for stars in 31 RLQ fields. Typically the robust star-galaxy separation limit is $K_{classlim}=17.5-18$, hence the dropoff in star counts fainter than that. Stars at $K_s>20$ were classified from snapshot *HST* images. Figure 9 shows the $K_s/r-K_s$ CMD for galaxies in 30 RLQ fields, with upper and lower limits and error bars omitted for clarity. A galaxy with a flat spectrum in f_ν has $r-K_s=2.06$ with our adopted zeropoints (see Appendix A of Paper 1 and Djorgovski *et al.* 1995).

We have statistically corrected the number-magnitude relation at $K_s>K_{classlim}$ for unidentified faint stars, but how do we statistically account for them in comparing quasar-field and control-field CMDs? Stars have a bluer mean $r-K_s$ color than galaxies, and thus could bias comparisons between fields at different Galactic latitude (and longitude). We could assume that stars uniformly populate the color range $r-K_s=1-4.5$. However, our $K_{classlim}$ values are faint enough that stellar contamination is only a $\sim 5\%$ effect at fainter magnitudes. We thus make no correction for stellar contamination in our consideration of CMDs, but will discuss the effects of it where relevant.

3.1. One-Dimensional Histograms

One simple method of comparing CMDs is to split them into different magnitude bins and compare the color histograms in each bin. In the following discussion we exclude the fields of Q 1508–055 (no r data), Q 2230+114 (nonphotometric R_C data), and Q 0736–063 (uncertain stellar contamination). At the 0^m5 binning size we use, the $\sim 0^m08$ difference between our conservative and liberal magnitude scales is not significant, so we adopt the latter. In Figure 11 we plot the surface density of galaxies, binned by $r-K_s$ color, from all 30 good RLQ fields (solid lines) and in the combined opt-IR control fields (dotted lines) discussed in Appendix A. Smaller histograms represent those galaxies with lower or upper limits to their colors. At $K_{UKIRT}\gtrsim 18$, there is a clear excess of red galaxies with $r-K>5$ in the quasar fields. This color and magnitude range is where we would expect to see bright cluster ellipticals associated with the quasars.

To quantify the significance of any difference between the color distributions regardless of surface density, taking into account upper and lower limits, we normalize all histograms separately to unit sum and use the Peto & Prentice Generalized Wilcoxon Test as implemented in the IRAF⁴/STSDAS task STATISTICS.TWOSAMPT. The two $r-K$ distributions are different at only 67% (1σ) significance at $K_{UKIRT}=17-18$, but at 99.98% (3.7σ) significance at $K_{UKIRT}=18-19$

⁴The Image Reduction and Analysis Facility (IRAF) is distributed by National Optical Astronomy Observatories, operated by the Association of Universities for Research in Astronomy, Inc., under contract to the NSF.

and at $>99.995\%$ ($>4\sigma$) significance in the faintest two bins shown, and at $K_{UKIRT}>21$ (not shown) for the handful of fields that reach that deep. Thus the excess galaxy population in these RLQ fields has a redder $r-K$ color distribution than the field population at $>99.995\%$ ($>4\sigma$) significance. Random field to field variations in $r-K$ color distributions are possible due to variations in galaxy population with environment, but should average out over many fields. Thus the excess population of predominantly red galaxies must somehow be connected with the presence of RLQs in our fields.

The red galaxy excess persists at $K_{UKIRT}=20-21$, in which magnitude range there is a significant deficit of blue galaxies. This apparent deficit is difficult to understand, since the $K_{UKIRT}\sim 20.5$ faint blue galaxy population is mostly at $z<1$ and should be uncorrelated with the presence of $z>1$ quasars in these fields. If foreground galaxy structures cause magnification bias in these fields, one might expect slightly fewer blue (late-type) galaxies in the fields due to the tendency of red (early-type) galaxies to preferentially inhabit denser environments, but this tendency is too weak to explain a complete absence of blue galaxies or why it occurs only in the faintest magnitude bin. In addition, the Butcher-Oemler effect (Butcher & Oemler 1984) is seen in clusters to $z\sim 1$ (Rakos & Schombert 1995; Lubin 1996), so it is natural to expect that these candidate $z=1-2$ clusters should also have a large ($\sim 40\%$) fraction of blue galaxies.

However, this apparent deficit is also difficult to explain away as spurious. There is adequate control field data (~ 200 galaxies) at $K_{UKIRT}=20-21$ from our control fields and the Hubble Deep Field IRIM (HDF-IRIM), Moustakas, and Djorgovski datasets. It is possible that conversion of the HDF-IRIM and Moustakas V and I magnitudes to r causes part of the offset between quasar- and control-field histograms, but the full $\sim 0^m.5$ offset is inconsistent with the scatter in the conversion (Eq. A) and the good agreement between control-field datasets obtained with different optical filters (Figure 10). More subtle errors involving different instruments and different magnitude measurement techniques cannot be ruled out, but the two largest control field datasets in this magnitude range were both obtained on the KPNO 4m with IRIM and catalogued using FOCAS total magnitudes and isophotal colors. Using our conservative magnitude scale reduces the deficit only slightly. The apparent deficit is of objects with $r=22-24$ and $K_{UKIRT}=20-21$, which is well above the detection limits for the r data but within $\sim 0^m.5-1^m.0$ of our 3σ K_s limits. The Eddington bias (Eddington 1913), the systematic overestimate of faint object fluxes due to the increase in number counts with decreasing flux, should only bias our K_s magnitudes brightwards by $\sim 0^m.1-0^m.2$ at our 5σ K_s limits, using Eq. 7 of Hogg & Turner (1997). However, this error will occur in our control fields as well, and they still show an excess of blue galaxies compared to our quasar fields. Any further systematic errors in our magnitude measurements are likely to exist only at our faintest limits (i.e. affecting only the K_s magnitudes of any “missing” objects) and to *underestimate* the magnitudes of faint objects (e.g. if FOCAS total magnitudes underestimate the flux for the lowest S/N objects compared to brighter objects). However, any such errors in K_s would produce a bias toward bluer $r-K_s$ colors, the opposite of what is observed, and would also occur in our control fields as well as quasar fields. Lastly, there is no significant deficit of galaxies

blue in $J-K$ at $K=19-20$ or $K=20-21$ in our data compared to the HDF-IRIM control field data. This suggests that the error occurs either in r or in both J and K_s if it is a straightforward magnitude measurement error, but we suspect it is instead due to a combination of errors. In any case, the excess of red galaxies at $K_{UKIRT}=20-21$ is still significant even if we arbitrarily shift the quasar- and control-field $r-K$ color histograms so that they match at the blue end.

In Figures 12 and 13 we plot the surface density of galaxies in each color bin for the $z<1.4$ and $z>1.4$ subsamples separately. The $z<1.4$ subsample is noisier, as usual, and is only useful down to $K_{UKIRT}=20$. The red galaxy excess is definitely present at $K_{UKIRT}=19-20$, and perhaps at $K_{UKIRT}=18-19$ as well. The $z<1.4$ and control field distributions are different at the 99.71% (3σ) significance level at $K_{UKIRT}=18-19$ and at the >99.995% ($>4\sigma$) level at $K_{UKIRT}=19-20$. The $z>1.4$ and control field distributions are different at the 99.99% (3.9σ) significance level at $K_{UKIRT}=18-19$, and at the >99.995% ($>4\sigma$) level at $K_{UKIRT}=19-20$ and $K_{UKIRT}=20-21$.

In Figure 14 we plot the fractional $r-K$ color distributions for galaxies at $\theta<40''$ (solid line) and $\theta>40''$ (dotted line) from the quasars. There is no significant difference between the histograms. The similarity between the color distribution of the excesses at small and large radii suggests that the large-scale galaxy excess is the same population as the $\theta<40''$ excess.

As a check on the reality of the redness of the excess population, we can plot the $K_{UKIRT}/J-K_{UKIRT}$ CMD for the five fields with J data. Figure 15 shows the $K/J-K$ control field CMD (see Appendix A), and Figure 16 shows the $K/J-K$ CMD of the five $z>1.4$ RLQ fields. Comparing the two, there appears to be an excess of galaxies in the RLQ fields with $K\gtrsim 19$ and $J-K\gtrsim 2$. In Figure 17 we plot the normalized $J-K$ color histograms in four magnitude bins. The $J-K$ distributions are not significantly different at $K<19$. They are different at the 98.28% confidence level (2.4σ) at $K=19-20$ and at the >99.995% ($>4\sigma$) level at $K=20-21$, in both cases due to the tail at $J-K\gtrsim 2$ in the RLQ fields. Only the HDF-IRIM dataset has J data for objects at $K>20$. (Note added in proof: the recent data of Bershad, Lowenthal & Koo (1998) has a $J-K$ distribution at $K_s=20-21$ consistent with HDF-IRIM.) Thus there is some evidence that the excess galaxy population is redder than the field population in $J-K$ as well as $r-K$. This more subtle difference is not surprising since even to $K=20$ most galaxies are at $z\leq 2$ (Cowie 1996) and the red envelope of $J-K$ colors for early-type galaxies increases only slowly out to that redshift.

3.2. Summary: Color-Magnitude Diagrams

The $r-K$ color distribution of the faint excess galaxy population is significantly redder than that of the field population. The $J-K$ color distribution for the five quasar fields with J data also shows a red tail not present in the field. There is no significant difference between the color distributions of the $\theta<40''$ and large-scale excess components. The colors and magnitudes of both excess populations are thus consistent with a population of predominantly early-type galaxies at the quasar redshifts. There is an apparent deficit of blue galaxies in the faintest magnitude bins

which is difficult to understand as either a real effect or a single systematic error. However, the red galaxy excess is still significant if we arbitrarily adjust the $r-K$ color histograms so as to eliminate the apparent deficit.

4. Estimates of Cluster Richnesses

We have seen that there is a significant faint galaxy excess in our RLQ fields with a color distribution redder than that of the field population. While only spectroscopy can determine the redshift distribution of the galaxy excess for certain, its magnitude, color, and spatial distributions are consistent with it being composed of clusters or other large structures at the quasar redshifts. We now assume that this is the case in order to quantify the richnesses such clusters would have.

Since we have no information on the dynamical state of these structures, our use of the term “clusters” can be somewhat misleading. Spectroscopy is needed to confirm or deny the hypothesis that these structures are virialized or virializing. Even then, the evolution of individual galaxies and clusters from $z>1$ to $z\sim 0$ might make accurate comparison with low-redshift clusters difficult without detailed comparison with simulations to identify similar populations of objects at each z . We discuss these and similar issues further in §4.3, but for now we assume the strength of the galaxy excess in our fields can be compared more or less directly with that of low-redshift clusters.

Abell (1958) defined a cluster’s richness as the number of member galaxies above background no fainter than 2^m0 below the third brightest cluster galaxy and within $1.5h^{-1}$ Mpc of the center. This criterion is difficult to apply directly at high z due to the large and uncertain background correction required over $3h^{-1}$ Mpc diameter and also to the uncertainty in identifying the third brightest cluster galaxy. Thus we use the alternate richness measurement $N_{0.5}$.

4.1. The Hill & Lilly Statistic $N_{0.5}$

Hill & Lilly (1991) defined the quantity $N_{0.5}$ to be the number of galaxies above background located within 0.5 Mpc radius of the quasar and with magnitudes between m_{BCG} and $m_{BCG}+3$, where m_{BCG} is the brightest cluster galaxy magnitude. This is similar, but not identical, to the $N_{0.5}$ used by Bahcall (1981). To measure $N_{0.5}$ in our data, we need to know $m_{BCG}(z)$. Also, for valid comparison with results at low z , we must account for redshift-dependent changes in the bright end of the galaxy luminosity function (between m_{BCG} and $m_{BCG}+3$).

4.1.1. What is $m_{BCG}(z)$?

Hill & Lilly (1991) were studying the environments of radio galaxies at $z\sim 0.5$, and so originally defined $m_{BCG}(z)$ to be the magnitude of the radio galaxy in each field. We choose to

define $m_{BCG}(z)$ as the magnitude given by the $K-z$ relation for high- z powerful radio galaxies (HzPRGs), supplemented by the $K-z$ relation of known BCGs at $z < 1$ (see §4.1.2). Assuming for the moment that HzPRGs are BCGs (see below for a discussion of this point), this has the advantage of having “built-in” evolutionary, cosmological, and k - corrections to the BCG magnitudes. In addition, the HzPRG population at $z=1-2$ does not show much more scatter in the $K-z$ relation than reasonably expected from studies of dozens of BCGs in clusters at $z \leq 0.05$ (Eales *et al.* 1993; Thuan & Puschell 1989; Postman & Lauer 1995).

One concern with estimating the BCG $K-z$ relation from that of HzPRGs is contamination of the K -band light either through scattered or direct AGN light or through AGN-induced star formation or line emission. Roche, Eales & Rawling (1997) examined 10 $z=1-1.4$ 6C radio galaxies (RGs), and found they have significantly smaller K' -band half-light radii than 3C RGs at similar z . Thus the brighter K magnitudes of the 3C galaxies are due, at least in part, to their larger sizes rather than an increased contribution by AGN-related flux. Best, Longair & Röttgering (1997; 1998) present several other arguments in favor of 3C RGs being BCGs. They claim a $\lesssim 15\%$ AGN-related contribution to the K -band light, and radial intensity profiles well matched by an $r^{1/4}$ law, both consistent with starlight from old populations dominating at K . In addition, the combined 3C RG K -band profile shows evidence of excess emission at $r > 35$ kpc, which they interpret as cD-type halos. A similar excess of K -band emission at large radii in 3C RGs relative to a sample of MG radio galaxies was found by McLeod (1994), who however suggested it may be due to very nearby (i.e. interacting) galaxies. There is also some direct evidence that at least some 3C RGs at $z > 1$ lie in clusters, as expected for BCGs. Dickinson (1997) has spectroscopically confirmed a cluster around 3C 324 at $z=1.206$ from which X-ray emission has also been detected (Smail & Dickinson 1995), and Deltorn *et al.* (1997) have spectroscopically confirmed a cluster around 3CR 184 at $z=0.996$. Extended cluster-scale X-ray emission has also been detected around several 3C RGs by Crawford & Fabian (1996a; 1996b).

A second issue in determining $N_{0.5}$ is whether the galaxy luminosity function (LF) down to $m_{BCG}+3$ has the same redshift evolution as m_{BCG} (BCGs are about 2^{m5} brighter than L^*). If not, then our values of $N_{0.5}$ may be biased with respect to low-redshift measurements. Best, Longair & Röttgering (1998, their Figure 1) show that at $z=1-2$ the $K-z$ relation for 3C RGs runs slightly brighter than the relation for a nonevolving elliptical normalized to 3C RGs at $z < 0.6$. From nearly complete redshift surveys, Cowie (1996, his Figure 2) shows that at all $z < 2$ the upper envelope of the field galaxy population’s K magnitude distribution tracks the same nonevolving elliptical $K-z$ relation (what Cowie plots is the $K-z$ relation of a nonevolving Sb galaxy with $M_K = -25.8$, but the two relations are very similar at $z=1-2$). In addition, Cowie *et al.* (1996) estimate the K -band LF and find, within the uncertainties, an invariant M_K^* and α to $z=1$ and consistency with an invariant M_K^* at $z=1-1.6$. These results show there must be some evolution in the BCG and field galaxy populations since neither are ever quite as bright at $z=1-2$ as the $K-z$ relation for passively evolving single-burst galaxies with $z_f=5$. However, since both populations agree reasonably well with a single $K-z$ relation (that of a nonevolving elliptical),

differential evolution between them is likely to be small at $z=1-2$, and so our $N_{0.5}$ values should not be strongly biased compared to ones made at low redshift.

4.1.2. The $K-z$ Relation for Powerful Radio Galaxies at $z=1-2$

To use the $K-z$ relation for HzPRGs to define m_{BCG} in our quasar fields, we must fit a function to that relation. We use the data on HzPRGs presented in Figure 3 of Eales *et al.* (1993), which have been corrected to 34.5 kpc apertures assuming $h=0.5$, the data of Arag3n-Salamanca *et al.* (1993), who give K_{CIT} magnitudes measured within a 50 kpc diameter aperture for 19 BCGs in optically selected clusters at $z<1$, and data for the two spectroscopically-confirmed $z>1$ BCGs (Dickinson 1995; Stanford *et al.* 1997). Fitting the combined data, we find

$$K = (17.12 \pm 0.06) + (5.10 \pm 0.11)\log(z) \quad (1)$$

with standard deviation 0^m37 . This relation is consistent with Figure 3 of Eales *et al.*. We adopt Equation 1 as describing the magnitudes of BCGs to $z=2$.

4.2. Calculating the Hill & Lilly Statistic $N_{0.5}$

We assume $H_0=75$, $q_0=0.1$, and $\Lambda=0$ to calculate $\theta_{0.5}$, the angular distance corresponding to $0.5h_{75}^{-1}$ Mpc at the quasar z , for each quasar. In each field we extract all galaxies inside and outside of $\theta_{0.5}$ between K_{BCG} (as given by Eq. 1) and $K_{BCG}+3$. However, only six fields have 5σ limits that reach $K_{BCG}+3$. (Our $z>1.4$ data reaches an average of $K_{BCG}+2^m42$, while our $z<1.4$ data reaches an average of $K_{BCG}+2^m05$.) For each other field, we scale the $N_{0.5}$ measurement down to $K_{5\sigma}$ to the expected value down to $K_{BCG}+3$ using measurements to both limits in the six deepest fields, suitably averaged. This eliminates the bias toward lower $N_{0.5}$ observed in the raw measurements to $K_{5\sigma}$ in these fields. The uncertainties on $N_{0.5}$ are dominated by the uncertainties in the background subtraction. There is no way to reduce the uncertainty on the number of galaxies within 0.5 Mpc between K_{BCG} and $K_{BCG}+3$, but the uncertainty on the background subtraction can be reduced by observing larger areas.

The results (for our liberal magnitude scale) are shown in Figure 18. The plotted error bars do not include the uncertainties in the corrections for fields which do not reach $K_{BCG}+3$. The average $N_{0.5}$ value lies above zero since we observe an excess near the quasars. However, the uncertainties are large: the average $N_{0.5}$ for all 31 good fields is 11.8 ± 12.0 , for all 20 $z>1.4$ fields is 11.4 ± 12.8 , and for all 11 $z<1.4$ fields is 12.5 ± 11.0 . Using the relations between $N_{0.5}$, B_{9q} , and Abell richnesses given in Hill & Lilly (1991), these $N_{0.5}$ values correspond to richnesses of Abell class 0 ± 1 , where by -1 we mean the richness of the general field. In other words, the 1σ upper limit on the average *near-field* richnesses of our quasars is Abell richness class 1, not including the uncertainty on the correction to $K_{BCG}+3$ where needed. By *near-field* we mean the galaxy

overdensity in the central $0.5h_{75}^{-1}$ Mpc radius region compared to the region beyond $0.5h_{75}^{-1}$ Mpc in our own data. This same Abell richness class 0 ± 1 result was found for 17 $z=1-1.4$ 5C and 6C radio galaxies by Roche, Eales & Hippelein (1997). In Figure 19 we plot the histogram of near-field $N_{0.5}$ values for all 31 fields. This plot can be directly compared with Figure 9 of Hill & Lilly (1991). Like FR II radio galaxies at $z\sim 0.5$ (their Figure 9a) and RLQs at $z\sim 0.5$ (their Figure 11), our quasars at $z=1-2$ show values extending from ~ 0 to ~ 40 , with an average greater than zero (typical Poisson uncertainties on our points are ± 2 bins).

We now consider the *far-field* richness, which we define as the galaxy overdensity in the central $0.5h_{75}^{-1}$ Mpc radius region compared to the literature expectation. We calculate these values in the same manner as the near-field richnesses, using the average published literature $N(m)$ and RMS in the appropriate magnitude range. The uncertainties are difficult to reduce other than possibly through a more accurate determination of the random-field RMS and through observing all fields to $K_{BCG}+3$. The results (for our liberal magnitude scale) are shown in Figure 20. These plotted error bars *do* include the uncertainties in the corrections for fields which do not reach $K_{BCG}+3$. The average far-field $N_{0.5}$ is larger than the average near-field $N_{0.5}$, as expected. The uncertainties are still large: the average far-field $N_{0.5}$ for all 31 good fields is 25.2 ± 19.1 , for all 20 $z>1.4$ fields is 28.8 ± 21.4 , and for all 11 $z<1.4$ fields is 16.4 ± 12.5 . This roughly corresponds to Abell richness 1.5 ± 1.5 for the $z>1.4$ subsample, and Abell richness 0.5 ± 1.0 for the $z<1.4$ subsample. Thus while the average richness levels are higher when compared to the literature expectation, the uncertainties are also larger due to the large field-to-field RMS seen in the literature.

The average “near-field” $N_{0.5}$ value for our two control fields is 5.6 ± 8.9 , calculated assuming $z=1.201$ and 1.315 for them so that their 5σ K limits are equal to $K_{BCG}+3$. Their average “far-field” $N_{0.5}$ value is -13.3 ± 10.3 with the same assumptions. This negative value is expected since our control fields’ galaxy counts are below the published literature average (Figure 9 of Paper 1). These control field results show no evidence for any systematic bias in our $N_{0.5}$ measurements.

4.3. Summary and Discussion: $N_{0.5}$

Under the assumption that the excess galaxies are all at the quasar redshifts, and that a straightforward comparison of $N_{0.5}$ values can be done between these quasars’ galaxy excesses at $z=1-2$ and clusters at $z\sim 0$, the values of $N_{0.5}$ we calculate indicate the *near-field* excess within $0.5h_{75}^{-1}$ Mpc ($\sim 65''$) around the quasars corresponds to Abell richness class $\sim 0\pm 1$, where by -1 we denote the richness of the field. This near-field excess is calculated with respect to our own data at $>0.5h_{75}^{-1}$ Mpc. We also measure the excess within $0.5h_{75}^{-1}$ Mpc compared to the expected literature counts; this *far-field* excess corresponds to Abell richness class $\sim 1.5\pm 1.5$. The excess across our entire RLQ fields (i.e. to beyond $0.5h_{75}^{-1}$ Mpc) compared to the expected literature counts is presumably part of the same overdensity as the far-field excess. At some $\theta \gtrsim 100''$ we expect that this overdensity will disappear and our counts will match the literature.

Could the excess galaxies be associated with intervening Mg II absorption-line systems? Such systems would have to be at $z \gtrsim 0.9$ to explain the colors of the excess galaxies. From Paper 1, intervening absorber information is available for only 4 objects at $z < 1.4$, but for 16 objects at $z > 1.4$. There are 8 $z > 1.4$ RLQs with known intervening absorption (14 $z > 0.9$ Mg II absorbers with $\bar{z} = 1.33 \pm 0.25$) and 8 $z > 1.4$ RLQs without it. These two subsamples have $< 1\sigma$ differences in their near- or far-field $N_{0.5}$ values despite this $\sim 3.5\sigma$ difference in the number of intervening absorbers along the line of sight. Although the statistics are admittedly small, there is no evidence that intervening Mg II systems contribute significantly to the galaxy excess. This is consistent with some published evidence that Mg II and C IV absorbers may tend to avoid clusters (Bechtold & Ellingson 1992; Morris *et al.* 1993; Ellingson *et al.* 1994). On the other hand, there is also evidence for excesses of galaxies at the redshifts of strong Mg II and/or damped Ly α absorbers from narrow-band imaging emission-line searches (Bunker *et al.* 1995; Francis, Woodgate & Danks 1997; Bechtold *et al.* 1998; Mannucci *et al.* 1998; Teplitz, Malkan & McLean 1998).

One simple interpretation of this result is that RLQs at $z = 1-2$ are located on a large scale ($\gtrsim 0.75h_{75}^{-1}$ Mpc) within clusters and/or large scale galaxy structures of Abell richness 0 or greater (1σ lower limit). On a smaller scale ($\lesssim 0.5h_{75}^{-1}$ Mpc) within those structures, the RLQs can be located in environments ranging from the field to clusters up to Abell richness 1 (1σ upper limit).

However, as mentioned in §4, the evolution of individual galaxies and galaxy clusters may complicate such comparisons. The numerical simulations of Steinmetz (1997) show that present day L^* galaxies typically have several progenitors at $z \sim 3$ spread over a few hundred kpc, and Sawicki & Yee (1998) find that the inferred total stellar masses of Lyman-break-selected $z \gtrsim 2$ galaxies in the Hubble Deep Field are not large enough for them to be the direct progenitors of L^* galaxies. If we assume that a present-day L^* galaxy has on average two progenitors at $z \sim 1-2$, then our richness measurements will be biased high by a factor of two on average. On the other hand, early-type galaxies in clusters or other dense structures may be fully formed at higher redshifts than field galaxies, while clusters are probably not fully formed at high z and so the galaxy excess in our fields may need to be counted within a larger radius for direct comparison with low redshift cluster richness measurements. This illustrates the need for detailed comparison of high-redshift observational data with numerical simulations in order to relate such objects to their better understood low-redshift counterparts. However, the above considerations will not change our basic finding that $z = 1-2$ RLQs are often embedded in large-scale galaxy structures and occasionally also in smaller structures the size of present-day groups or clusters. (See §8 for a discussion of these structure’s richnesses in a broader context.)

As large as the uncertainties on $N_{0.5}$ are, the near-field $N_{0.5}$ values would have had even larger uncertainties if we had not designed our data reduction procedure to make use of the edges of the fields which have less than the full exposure time. More accurate determination of RLQ richnesses at $z = 1-2$ will require data down to $m_{BCG} + 3$ over wider fields ($> 4' \times 4'$). Such imaging might best be done in J or H if their field-to-field galaxy RMS is smaller than in K .

5. The K -band Luminosity Function of Candidate $z>1$ Galaxies

We have shown that an excess of red galaxies exists in our fields, that the color distribution of the excess at $\theta < 40''$ from the quasars is indistinguishable from that at $\theta > 40''$, and that the color and magnitude distributions of the excess galaxies are broadly consistent with them being galaxies at the quasar redshifts. Our data are too noisy for us to fully constrain the luminosity function (LF) of the excess population under this assumption, but we can put some constraints on M_K^* . First, some terminology: K_{BCG} is the apparent K magnitude for brightest cluster galaxies (BCGs), M_K^{BCG} is the BCG absolute K magnitude, M_K^* is the absolute K magnitude of the knee in the luminosity function, and K^* is the apparent K magnitude of the knee.

The usual method used to determine the LF is to assume a cosmology and a prescription for k -corrections, use them to determine absolute magnitudes for the excess galaxies, and fit a Schechter function to the resulting absolute magnitude distribution. However, since our fields reach only $\sim 2^m 5$ below K_{BCG} on average, we are not sensitive to (and cannot constrain) the faint-end LF slope α . Similarly, since we do not know the volume over which the excess galaxies are distributed, we cannot constrain the LF normalization ϕ^* .

We assume our usual cosmology of $H_0=75 \text{ km s}^{-1} \text{ Mpc}^{-1}$, $q_0=0.1$, and $\Lambda=0$. For our no-evolution k -correction we adopt the average of the K -band k -corrections for the 15 Gyr old model E and Sa galaxies of Poggianti (1997). At the relevant rest wavelengths ($\lambda > 6600 \text{ \AA}$), these k -corrections change very little over redshifts $z=1-2$ and ages 11–15 Gyr. We count all galaxies across each field brighter than the 5σ K limit ($K_{5\sigma}$), correct for incompleteness, subtract the expected literature counts, calculate absolute magnitudes assuming the excess galaxies are all at the quasar redshifts, sum up the individual fields' excesses, and normalize by the area in each absolute magnitude bin. We ignore the faintest bin since it contains data from only one field.

The results for $z < 1.4$ and $z > 1.4$ on our liberal magnitude scale are the solid lines in Figure 21 and Figure 22, respectively, with dashed lines the $\pm 1\sigma$ Poisson uncertainty ranges. In our cosmology our assumed K_{BCG} (Eq. 1) corresponds to $M_K^{BCG} = -26.56 \pm 0.36$ (including intrinsic dispersion of $0^m 3$) at $z=1.4-2$, and -26.28 ± 0.31 at $z=1-1.4$. Thus the $< 2\sigma$ excess at $M_K < -27$, which consists of only a few observed galaxies, is almost certainly not at the quasar redshifts.

We fit the observed excess $N(M_K)$ with a Schechter function, defined as

$$\phi(M) = 0.92\phi^* \exp(-0.92(M - M^*)(\alpha + 1) - \exp[-0.92(M - M^*)]) \quad (2)$$

(Schechter 1976). Most previous K -band LF determinations find $\alpha = -1.0$ within their uncertainties, and Eq. 2 reduces to

$$\phi(M_K) = 0.92\phi^* \exp(-\exp[-0.92(K - K^*)]) \quad (3)$$

To estimate K^* , we simply assume various values of K^* , generate $\phi(M_K)$ for each, and shift this curve vertically by the weighted difference between it and all bins fainter than $M_K = -26.5$ since ϕ^* is unconstrained. Objects brighter than $M_K = -26.5$ are very unlikely to be at the quasar

redshifts. Bins fainter than $M_K = -23.5$ in the $z=1-1.4$ subsample are excluded due to their large uncertainties. The χ^2 for this shifted curve compared to the data is calculated and the procedure repeated for different K^* to find the value which yields the lowest χ^2 . The result is $M_K^* = -25.25_{-\infty}^{+1.10}$ for our $z=1-1.4$ fields and $M_K^* = -24.85_{-0.50}^{+0.35}$ for our $z=1.4-2$ fields. The $\pm 1\sigma$ limits are the values of $K^* - K_{BCG}$ which yield $\pm 1\sigma$ deviant χ^2 values.

5.1. Discussion

We compare our results with the LF of Gardner *et al.* (1997): $M_K^* = -23.90 \pm 0.10$ at $\bar{z} = 0.14$. Gardner *et al.* measure magnitudes in $10''$ diameter apertures (Gardner *et al.* 1996), or 22 kpc diameter at $\bar{z} = 0.14$ for our cosmology. This is equivalent to a $3''$ diameter aperture at $z=1-2$, smaller than the typical total magnitude aperture for our faint galaxies, but comparable to the typical isophotal magnitude aperture. The average offset between these two magnitudes is $\sim 0^m.3 \pm 0^m.2$ (see Figure 4 of Paper 1). Since our magnitudes are probably systematically brighter than those of Gardner *et al.* by roughly this amount, we include this offset and uncertainty in our luminosity evolution estimates. Our results are consistent with mild luminosity evolution, or none: $-1.05_{-\infty}^{+1.12}$ magnitudes in 11 RLQ fields with $\bar{z} = 1.13$ and $-0.65_{-0.55}^{+0.41}$ in 20 RLQ fields with $\bar{z} = 1.67$. We stress that these estimates are made assuming that all excess galaxies in these fields are at the quasar redshifts and with a very simple fit to an arbitrarily normalized Schechter function with fixed faint-end slope. Nonetheless, a somewhat more empirical estimate of luminosity evolution from $\phi(K - K_{BCG})$ agrees well with our estimate from $\phi(M_K)$. In addition, this is roughly consistent with passive evolution of stellar populations formed at high z : Poggianti (1997) give passive evolution of -1.05 ± 0.10 and -1.33 ± 0.12 magnitudes to the same redshifts for an equal mixture of Sa and E galaxies in an $H_0 = 50$, $q_0 = 0.225$ universe.

If the excess galaxies were consistently located foreground to the quasars, our estimates of their absolute magnitudes would be biased systematically bright. To erase the evolution seen in M_K^* the excess galaxies would need to have $\bar{z} = 0.7$ in the $\bar{z} = 1.13$ RLQ sample, and $\bar{z} = 1.2 \pm 0.1$ in the $\bar{z} = 1.67$ RLQ sample. This is more or less independent of the assumed cosmology. We can rule out $\bar{z} \sim 0.7$ since galaxies at that redshift would not show such a strong tail to very red colors in $r - K$. We cannot rule out $\bar{z} \sim 1.2$ since galaxies can be as red as $r - K \sim 6$ at that redshift. Thus our detection of luminosity evolution in M_K^* from $\phi(M_K)$ is quite dependent on our assumption that the excess galaxies are all at the quasar redshifts. However, if the excess galaxies are at $z \gtrsim 0.9$ as indicated by their $r - K_s$ color distribution, the most likely redshift for them to be at is the quasar redshift, since there is no evidence that intervening Mg II systems contribute significantly to the galaxy excess (§4.3) and the only other reason for an excess galaxy population in many fields would be weak lensing amplification of these $z=1-2$ RLQs, but large scale structure at $z \gtrsim 0.9$ would not efficiently cause such an effect.

To summarize, in our adopted cosmology observed K -band BCG magnitudes match no-evolution predictions to within $0^m.3$. Assuming the excess galaxies are at the quasar redshifts,

we estimate $-1.05_{-\infty}^{+1.12}$ magnitudes of luminosity evolution to $\bar{z}=1.13$ and $-0.65_{-0.55}^{+0.41}$ to $\bar{z}=1.67$. If our assumed cosmology is in error, the amount of passive evolution we infer will also be wrong; a $q_0=0.5$ cosmology would reduce our estimated luminosity evolution by $\sim 0^m3$.

5.2. Comparison with Previous Work

Our result is broadly consistent with previous work. Studies of the K -band LF through various means exist at low redshift (Mobasher, Sharples & Ellis 1993; Glazebrook *et al.* 1995; Gardner *et al.* 1997), in a $z=0.3$ cluster (Barger *et al.* 1995), to $z\sim 1$ (Aragón-Salamanca *et al.* 1993; Steidel, Dickinson & Persson 1994; Cowie *et al.* 1996), and at $z>1$ (Aragón-Salamanca *et al.* 1994; see also Aragón-Salamanca, Ellis & O’Brien 1996). We adopted the Gardner *et al.* M_K^* since it is the most accurate value to date and lies between those of the other two low- z studies.

From a $K<18$ field galaxy redshift survey, Elston (1994) suggested that $\sim 1^m$ luminosity evolution to $z\sim 1$ in bright early-type galaxies is required, in agreement with the results of the Lebofsky & Eisenhardt (1986) survey of a heterogenous sample of ellipticals and radio galaxies to $z=1$. However, Cowie *et al.* (1996) find from a $K<20$ field galaxy redshift survey that within their $\pm 0^m5$ uncertainties, M_K^* is invariant to $z=1$ and is consistent with being invariant at $z=1-1.6$, where they observe a deficit of bright galaxies ($M_K<-25.1$) despite $>95\%$ complete spectroscopy, which argues against a brighter M_K^* at $z>1$. From a Mg II absorption line selected galaxy sample, Steidel, Dickinson & Persson (1994) also find no evolution in the K -band LF to $z=1$.

The studies of Barger *et al.* (1995) and Aragón-Salamanca *et al.* (1993) found no evidence for evolution in M_K^* (within $\pm 0^m3-0^m4$ uncertainties) in clusters since $z=0.3$ and from $z=0.37$ to $z=0.9$, respectively. (The latter study did find evidence for color evolution of the reddest cluster galaxies consistent with passive evolution, however.) Also, Aragón-Salamanca *et al.* (1994) found that the LF of Mobasher, Sharples & Ellis (1993) was consistent (within uncertainties of $\pm 0^m45$) with that of a sample of candidate $z=1.3-2$ multiple C IV absorbing galaxies.

However, there is evidence for surface brightness evolution in both cluster and field early-type galaxies from the work of Schade and collaborators (Schade *et al.* 1995; Schade *et al.* 1996ab; Schade, Lopez-Cruz & Barrientos 1997; see Schade 1996 for a review). The amount of evolution at a given galaxy size is $\Delta M_B=-z$ in the rest-frame B -band to $z=1.2$. The simplest interpretation of the surface brightness evolution is luminosity evolution at a level consistent with passive evolution from formation at high z . There is no evidence for differential evolution between field and cluster early-type galaxies to $z\sim 0.6$, although the dense cluster cores are not well represented in the cluster sample. The results on cluster ellipticals are supported to $z\sim 0.4$ by other spectroscopic (van Dokkum & Franx 1996; Bender, Ziegler & Bruzual 1996) and imaging work (Barrientos, Schade & Lopez-Cruz 1996; Pahre, Djorgovski & de Carvalho 1996; Dickinson 1997).

Thus there is no clear consensus on the magnitude of luminosity evolution in galaxies to $z\sim 1$ (cf. Zepf 1997; Hudson *et al.* 1997; Brinchmann *et al.* 1998; Lilly *et al.* 1997). Such evolution

should be stronger in the blue, which may help reconcile the $1^{m}0 \pm 0.20$ rest-frame M_B evolution of Schade *et al.* with the $<0^{m}5$ limit on M_K evolution of Cowie *et al.*. Given the uncertainties, our results are not in conflict with previous work, but the excess population in our RLQ fields does suggest a brighter M_K^* at $z > 1$ than at $z = 0$, in contrast to the trends seen by Cowie *et al.* (1996) and Aragón-Salamanca *et al.* (1994), but in agreement with the work of Schade and collaborators.

6. Color Pictures

Although color pictures themselves cannot really be used for quantitative analysis, they are extremely useful for visualization, particularly for comparing the colors of galaxies in different fields. The IRAF COLOR.RGBSUN task was used to create Sun color rasterfiles for each field, which were converted to color PostScript using xv. The red, green, and blue images were the K_s , summed $r+K_s$ (or J when available), and r images. The images were not convolved to the same PSF, which leads to occasional spurious effects. The pictures have maximum intensities set to a common surface brightness in mag/pixel², so that a given color and brightness represents the same color and magnitude in every field, except for edge effects which arise because the normalized, constant-rms images were used to create the pictures.

Two notable fields are shown here. Even these high-quality plots do not really do justice to the color images, which can be better viewed on-line at <http://www.astro.utoronto.ca/~hall/thesis.html>. In both pictures North is at top, East at left, and the bright, blue quasar at center. Figure 23 shows the field of Q 0835+580 ($z=1.534$). There is a clump of very red ($r-K_s \gtrsim 5$) galaxies around the quasar (which is partially merged with a fainter star.) Figure 24 shows the field of Q 1126+101 ($z=1.516$). Of particular note are the faint orange- and red- colored galaxies to the WNW of the quasar (bright bluish-white object at center). These galaxies have similar, red $r-K_s$ colors, but the red-colored galaxies are also quite red in $J-K_s$, which makes them candidate background galaxies at $z \gtrsim 2.5$ (see §7.3). Also of note are the yellow-green objects $\sim 1'$ ESE and $\sim 2'$ NNE of the quasar. These objects have red $r-K_s$ (the ESE object is the reddest object in $r-K_s$ in any field) but blue $J-K_s$, which makes them candidate extreme late-type stars, although the NNE object may be extended.

7. Spectral Energy Distributions of Candidate $z > 1$ Galaxies

In fields where we have data in filters other than just r and K_s , it is worthwhile to compare the spectral energy distributions (SEDs) of red objects to models of evolving stellar populations to see how strongly the galaxy redshifts and/or stellar populations can be constrained. Our approach is a qualitative one since we have at most six points with which to constrain the SEDs and since many parameters of old stellar populations are uncertain at the $\sim 30\%$ level using current models (Charlot, Worthey & Bressan 1996; Spinrad *et al.* 1997).

7.1. The Candidate Group or Cluster Around Q 0835+580 (3C 205)

There is a fairly distinct clump of objects within $\sim 20''$ of Q 0835+580. The 19 catalogued objects to our 5σ K limit within $20''.5$ (excluding one star at $\theta=20''.39$) yield a surface density of ~ 47 galaxies per arcmin². One object is known to be at $z=0.236$, and one is unresolved on the WFPC2 snapshot of this field and is likely a star. Only one other shows up on the WFPC2 image, and it is definitely a galaxy. None of the others are likely to be stars since WFPC2 snapshots can detect unresolved objects to very faint limits. The compact spatial distribution of these galaxies, and the red color of many of them, makes it very likely that they are at the redshift of the quasar ($z=1.534$) or the intervening Mg II systems ($z\sim 1.4368$).

The two reddest objects at $\theta < 20''.5$ have 3σ lower limits to their $r-K_s$ colors of 7.03 (#339, $\theta=11''.25$) and 6.79 (#347, $\theta=10''.60$; this object is in fact an *riz* dropout with $\gtrsim 24^m.9$ in each filter, and is detected only in JHK_s .) We convert their magnitudes to F_ν and normalize to the same flux in K_s . These are plotted as the filled points and error bars in Figure 25, for *rizJHK_s* filters.

To fit these SEDs, we consider various model elliptical spectra at of the appropriate age for the assumed $z\sim 1.5$ of the galaxies, all normalized to the data at K_s . In our assumed cosmology the universe was 3.53 Gyr old at $z=1.534$, and is 11.06 Gyr old at $z=0$, slightly lower than the most recent post-Hipparcos globular cluster age estimate of 11.5 ± 1.3 Gyr (Chaboyer *et al.* 1998).

Exponentially declining star formation histories can adequately fit ellipticals at $z=0$, but cannot fit these galaxies if they are at the quasar redshift of $z=1.534$. This is shown by the dashed line in Figure 25, which is a 3.4 Gyr old elliptical (E) with an exponentially declining star formation rate with $\tau=1$ Gyr from Poggianti (1997). It fits the data at $\lambda > 4000\mu\text{m}$ in the rest frame, but is much too blue at $\lambda < 4000\mu\text{m}$. We consider models with a shorter star formation burst for a better fit. Specifically, we use the Bruzual & Charlot (1996) GISSEL96 spectral synthesis code to produce the spectrum of a solar metallicity E viewed 3 Gyr after the start of a 1-Gyr burst with a Scalo IMF from 0.1 to $125 M_\odot$, using the theoretical stellar spectra of Kurucz and Lejeune, Buser & Cuisinier (1996). However, this model (dotted line) still produces too much flux at observed z and possibly i ($< 4000 \text{ \AA}$ rest), even though it fits well at $\lambda > 4000 \text{ \AA}$. (The plotted error bars on the fluxes do not include systematic uncertainties, and so we attach little weight to the models' not matching the JHK data simultaneously.) As a check on the uncertainties in the stellar population modeling, we also use the PEGASE (Fioc & Rocca-Volmerange 1997) code to simulate a 1-Gyr burst solar metallicity E with Scalo IMF from 0.1 to $120 M_\odot$. Our (qualitative) results are unchanged if we use the PEGASE model elliptical, since for this spectral range and age it is essentially indistinguishable from the GISSEL model. Different stellar population models can often produce very different results (§7), so it is reassuring that our basic conclusions remain unchanged whichever of these two models we use.

To produce a stronger 4000 \AA break to match the observations, an older or a more metal-rich population is needed. Dust extinction will not produce the desired effect because the allowed reddening between 0.4–0.9 μm rest frame is smaller than the reddening needed at $< 0.4\mu\text{m}$ to

match the model with the data. Figure 26 shows that a 3 Gyr old 1-Gyr burst GISSEL model E reddened by $E(B-V)=0.25$ ($\tau_V \sim 0.7$) predicts only $\sim 60\%$ of the observed flux at J . The strength and abruptness of the break between z and J (observed) requires a strong 4000 Å break between those filters, either from age or metallicity.

A somewhat more speculative possible cause for the strong 4000 Å break is a nonstandard initial mass function (IMF) with a high low-mass cutoff $m_L \sim 1-5 M_\odot$ (Bithell & Rees 1990; Charlot *et al.* 1993). Depending on m_L , 4000 Å break amplitudes $\sim 20-40\%$ larger than those of normal ellipticals can occur over a period of $\lesssim 0.5$ Gyr for bursts containing 25–100% of the underlying galaxy mass. There is some evidence for high- m_L IMFs in some local starbursts (Engelbracht 1997; Charlot *et al.* 1993 and references therein). Determining whether a strong 4000 Å break is caused by a nonstandard IMF rather than high metallicity would require high S/N spectroscopy.

A 6 Gyr old 1-Gyr burst GISSEL model E (solid line in Figure 25) fits the data reasonably well at all observed wavelengths, but this is uncomfortably old for $z=1.534$. A ~ 5 Gyr old model with burst duration 0.1 Gyr fits similarly well, but 5 Gyr is still quite old for $z=1.534$. Worthey (1994) showed that two populations will appear almost identical if $\Delta T/\Delta Z=3/2$, where ΔT and ΔZ are the age and metallicity changes, in percent. In other words, the +100% change in the age of the universe at $z=1.534$ in our cosmology which we require to match the observed SEDs of these two objects could instead be produced by approximately a +67% (+0.21 dex) change in the metallicity. To test this, we use GISSEL96 to produce spectra for ellipticals formed in 1-Gyr bursts with metallicities $Z=Z_\odot$ ($[\text{Fe}/\text{H}]=+0.0932$) and $Z=2.5Z_\odot$ ($[\text{Fe}/\text{H}]=+0.5595$). The results are shown in Figure 27. The high-metallicity E (solid line) is as good a fit to the data as the 6 Gyr E model in Figure 25. Thus the SEDs of these objects are consistent with ~ 3 Gyr old metal-rich ellipticals, even though the metallicities of $z=0$ ellipticals averaged over the entire galaxy like our SEDs are likely to be roughly solar (Spinrad *et al.* 1997 and references therein).

However, these two objects are *redder* than LBDS 53W091 ($z=1.552$), a mJy radio source with $r-K \sim 6.15$ (Dunlop *et al.* 1996) whose ultraviolet spectrum is remarkably similar to M32. M32 is believed to contain an intermediate-age stellar population $\sim 4-5$ Gyr old in addition to the old stellar population usually present in ellipticals (Spinrad *et al.* 1997, and references therein). Spinrad *et al.* (1997) claim an age of $\gtrsim 3.5$ Gyr for LBDS 53W091, and Dunlop (1996) quote $\gtrsim 4.5$ Gyr for a similar galaxy (LBDS 53W069 at $z=1.432$). On the other hand, Bruzual & Magris (1997) claim that LBDS 53W091 can be modelled as an elliptical only 1–2 Gyr old if the full rest-frame 0.2–1 μm SED is taken into account, The discrepancy is partially due to the evolutionary spectral synthesis models they use (Bruzual & Charlot 1993), which produce red rest-frame $R-K$ colors as fast or faster than any other such models (Spinrad *et al.* 1997, Figure 16). However, it is also partially due to the rest-frame optical-IR colors of LBDS 53W091 being bluer than those of M32 despite the similarities in their rest-frame UV spectra. (Heap *et al.* (1998) also claim an age of ~ 2 Gyr for LBDS 53W091, on the independent basis of comparison with a Space Telescope Imaging Spectrograph ultraviolet echelle spectrogram of an F8V star.)

In Figure 28 we compare the SEDs of our two $r-K_s \sim 7$ objects to the spectrum of M32 (Bica *et al.* 1996), normalized at K_s . Within the systematic uncertainties, the M32 spectrum is a good fit. This is consistent with the good fit of the 6 Gyr model in Figure 25. The Bica *et al.* M32 agrees well with the 0.4–0.65 μm spectrum of Hardy & Delisle (1996), but is bluer than the “M32(b)” SED of Magris & Bruzual (1993). Even adopting the latter spectrum, however, the main objection of Bruzual & Magris (1997) to the old age claimed for LBDS 53W091 at $z \sim 1.5$ is substantially weaker for these two galaxies at similar z , and possibly for a third object with $r-K_s \gtrsim 6.5$ in the field (#618, $\theta = 99''$). Deep optical spectra of these objects have the potential of placing constraints on the cosmological model as strong as or stronger than those claimed for LBDS 53W091 by Spinrad *et al.* (1997).

The seven objects next reddest in $r-K_s$ at $\theta < 20''.5$ have $r-K_s = 4.95\text{--}5.80$. The remaining nine at $\theta < 20''.5$ — excluding the galaxy of known $z = 0.236$ — have $r-K_s = 2.68\text{--}4.49$, consistent with any $z \gtrsim 0.5$, and we do not consider them further. We normalize these objects to the same flux in K_s and compute the weighted average F_ν in each filter. We plot the average and RMS scatter in Figure 29 and compare to model spectra. The 3.4 Gyr old Poggianti E model produces too much flux in observed riz . A 2 or 3 Gyr old GISSEL model is a decent fit: the 3 Gyr old model (dotted line) fits best in z , and the 2 Gyr old model (solid line) fits best in i , but both predict too little flux in r . This can be interpreted to mean that, on average, star formation dropped off in these objects more quickly than an exponential but less quickly than a sudden cutoff of a burst. The inferred ages of these very red objects within $20''$ of 3C 205, and others at larger distances from the quasar, do not strongly constrain cosmological models. However, if they truly are younger than the extremely red objects (EROs) with $r-K_s \gtrsim 6.5$ discussed earlier and yet are also early-type galaxies at the same redshift, it would mean that $z \sim 1.5$ is near enough to the formation epoch of these galaxies for the dispersion in the rest frame $U-V$ colors of early-type galaxies to rise above the small values seen at $z \lesssim 1$ (Stanford, Eisenhardt & Dickinson 1998).

7.2. The Southern Radio Hotspot of 3C 205

Lonsdale & Barthel (1986; 1988; 1998) have studied the radio morphology of this quasar at VLBI resolution. The southern hotspot is extremely compact, curved, and polarized, and is located $2''.3$ W and $8''.2$ S of the quasar. One of the extremely red galaxies discussed above (#347) is located $3''.80$ W and $9''.89$ S of the quasar ($\theta = 10''.60$), consistent with the hotspot being produced by the collision of the radio jet with part of this galaxy. (There may be a small ($< 3^\circ$) rotation of our image relative to true north.) This “hotspot galaxy” has $K_s = 19.53 \pm 0.07$, $r-K_s > 6.79$ (3σ lower limit), $z-J > 3.89$ (3σ), $J-K_s = 1.87 \pm 0.06$, and $H-K_s = 0.85 \pm 0.18$. As we saw in §7.1, this object’s SED is red enough to match that of a metal-rich and/or very old galaxy, but its observed $> 1 \mu\text{m}$ slope does not allow much dust extinction. Thus the jet is probably being deflected by a high-pressure X-ray halo around the galaxy rather than dusty gas within it.

Could the hotspot object be synchrotron emission from the hotspot itself? The SED of such

emission is expected to have $f_\nu \propto \nu^{-1}$ (Ridgway & Stockton 1997), or $r-K_s=3.33$, $z-J=1.49$, $J-K_s=1.61$, and $H-K_s=0.81$. The near-IR colors of the hotspot object are consistent with the expected synchrotron emission, but such emission cannot explain the break at $\sim 1\mu\text{m}$, observed, which is most naturally explained as a 4000 \AA break at $z\sim 1.5$, consistent with the quasar redshift.

7.3. Candidate Associated and Background Galaxies in the Field of Q 1126+101

A very intriguing feature of the field of Q 1126+101 is that many of the $r-K_s > 4$ galaxies have very red $J-K_s$ colors as well (cf. the reddest objects in Figure 24). In this section we show that the SEDs of these objects are most consistent with either galaxies at $z \gtrsim 2.5$ (*background* to the quasar) whose 4000 \AA breaks lie between J and K_s , or with very dusty galaxies at the quasar redshift of $z=1.516$. Many of these objects have $r-K_s$ and $J-K_s$ colors similar to the spectroscopically confirmed $z=2.38$ galaxies of Francis, Woodgate & Danks (1997), and several are actually redder in $J-K$ than the only ERO with a spectroscopic redshift, HR10 (Hu & Ridgway 1994), which requires dust reddening in any reasonable cosmology to fit its SED at its known $z=1.44$ (Graham & Dey 1996; Cimatti *et al.* 1997).

We attempt only qualitative SED modelling, first trying to fit each object with elliptical spectra of reasonable age for the assumed z to minimize the required dust extinction. To model the effects of dust, we used the standard Milky Way (MW), LMC, and SMC extinction laws and the Calzetti (1997) law. The Calzetti formula was derived for active star-formation regions and empirically incorporates the “selective attenuation” effects of dust, including extinction, scattering, and geometrical dust distribution effects. In any case, the relative extinction from ~ 2500 to 9000 \AA (observed r to K at $z=1.5$) is similar for all four of these curves, as seen in Figure 30.

In Figure 30 we plot the two objects with $r-K_s > 5$ which are reddest in $J-K_s$ (#424 and #315). A 2.2 Gyr old $\tau=1$ Gyr Poggianti E at $z=2.5$ with $E(B-V)=0.35$ ($\tau_V \sim 1$) provides a good match to the SEDs of these objects. The choice of reddening law does not strongly affect the fit except at r and possibly at z . The break between J and H is suggestive of $z \sim 2.5$ for these two objects, but the lack of detected flux except at r and K_s makes for a weak constraint on the redshift. However, a lower redshift would require a larger τ_V since longer rest-frame wavelengths would be observed, and a younger galaxy or one with a more extended star-formation history would require more dust. The required reddening can be reduced to $E(B-V) \sim 0.25$ by fitting with a ~ 2 -Gyr old 1-Gyr-burst and a young ($\lesssim 0.1$ Gyr) population contributing substantial light only at $< 1\mu\text{m}$ (observed). Similar $E(B-V)$ values were found by Sawicki & Yee (1998) for confirmed $z > 2$ galaxies in the Hubble Deep Field (HDF) through detailed SED fits.

Figure 31 shows that the same $E(B-V)=0.35$ Poggianti E fits the J and K_s fluxes of the two objects with $r-K_s < 5$ which are reddest in $J-K_s$ (#18 and #237). However, these objects definitely require an additional young population to match the blue $r-J$ colors.

The lack of usefully deep H data for the above objects prevents firm redshift estimates. Our

assumed $z=2.5$ is the lowest that places the 4000 Å break redward of J , but while strong breaks in the objects’ spectra are consistent with the observed SEDs, they are not necessarily required. Figure 32 shows the only two objects with $J-K_s > 2.5$ with firm detections in H which might help better constrain their redshifts (#425 and #381). These objects are more consistent with dusty galaxies at the quasar redshift $z=1.516$ than objects at $z \sim 2.5$ due to the strong spectral break between z and J (compare to the objects in Figures 30 and 31 which cannot have such strong breaks). Such objects are unusual; there are only two other $J-K_s > 2.5$ galaxies which definitely have similarly strong breaks. The red $J-K_s$ and blue $r-z$ colors can be fit only with composite stellar populations, e.g. a dusty 2 Gyr old population with $E(B-V)=0.75$ ($\tau_V \sim 2$) and a young (100 Myr) dust-free population with $\sim 1\%$ of the total mass. The only way to avoid dust would be with metallicities $Z > 5Z_\odot$ and/or ages $\gtrsim 5$ Gyr, plus a young component providing flux in r .

7.4. Candidate Dusty Associated and/or Background Galaxies in Other Fields

The presence of candidate dusty galaxies around RLQs at $z \sim 1.5$ is relevant to the evolution of early-type galaxies in clusters and groups, and the surface density of candidate $z \gtrsim 2.5$ galaxies is interesting in its own right, so we briefly examine $J-K_s > 2.5$ objects in the other fields with deep J data (Q 0835+580, Q 0952+179 and Q 1258+404).

The surface densities of objects with $J-K_s > 2.5$ and $K < 21$ are 4.31 arcmin⁻² in the Q 1126+101 field and 1.90 arcmin⁻² in the other three fields. If we also require $r < 25.5$ the surface densities are 2.80 and 1.29 arcmin⁻² respectively, to $\pm 25\%$ accuracy. Whatever these galaxies are, the Q 1126+101 field is clearly unusual.

It is worthwhile to compare the surface density of these candidate $z \gtrsim 2.5$ “ J -dropouts” (objects with $J-K > 2.5$) with that of “ U -dropouts” at $z \sim 3.0 \pm 0.5$. From Steidel *et al.* (1998b), to $R_{AB}=25$ (or $r=25.5$) there is ~ 1 U -dropout/arcmin². The four U -dropouts with published K data have $K=21.3-22.1$ and $R_{AB}-K=2.7 \pm 0.5$ (Steidel *et al.* 1996). Thus, at the same r magnitude the surface densities of J - and U -dropouts are approximately equal, but our J -dropouts are about $\sim 2^m$ brighter in K and thus $\sim 2^m$ redder in $r-K$ than U -dropouts. This implies that many J -dropouts should be found among U -dropouts studied in the IR. Only four with $J-K > 2.5$ have been seen among the four objects mentioned above and the 17 U_{300} -dropouts in the HDF studied by Sawicki & Yee (1998). These results could be reconciled if faint $z \sim 2.5$ galaxies are on average redder than faint $z \sim 3$ galaxies, but if anything the opposite is seen by Sawicki & Yee (1998). To reduce the discrepancy between the inferred surface densities of J -dropouts at $z \gtrsim 2.5$ and U -dropouts at $z \sim 3$, we are led to the conclusion that a substantial fraction of our J -dropouts are not at $z \sim 2.5$ but are dusty galaxies at the quasar redshifts. Even then, the relative surface densities are such that we expect up to 50% of U -dropouts will be J -dropouts, larger than the $20 \pm 10\%$ seen to date among the 21 U -dropouts with published near-IR data.

This conclusion is consistent with the surface densities of J -dropouts in literature control

fields with J data (Appendix A). In 43.14 arcmin² to $K=21$ the surface density of $J-K_s>2.5$ galaxies is 0.46 arcmin⁻², about half that in our fields (excluding Q 1126+101). This suggests that roughly half our J -dropouts are in fact associated with the quasars.

The SEDs of our J -dropouts are also consistent with about half being dusty galaxies at the quasar redshifts z_q . Only Q 0835+580 and Q 1126+101 have z - and J -band data which is needed to identify the 4000Å break at $z_q\sim 1.5$. If we select $K_s<21$ objects with $J-K_s>2.5$ and $r-K_s>5$ (indicating a possible break between r and K_s), 7 of 22 such objects in the Q 1126+101 field and 7 of 10 in the Q 0835+580 field (roughly half in all) have $z-J$ colors or lower limits consistent with dusty galaxies at z_q .

7.5. Summary: Spectral Energy Distributions

There is a distinct overdensity of galaxies around Q 0835+580 (3C 205). The extremely red spectral energy distributions (SEDs) of the two reddest objects within $\sim 20''$ (and a third object $99''$ away) could be due to metallicities $\gtrsim +0.2$ dex above solar or to stellar populations as old as M32 (4–5 Gyr) at $z\sim 1.5$. Dust extinction cannot explain the entire SEDs due to the strong break between z and J (observed), presumed to be the 4000 Å break. The SEDs of the seven next reddest objects in $r-K_s$ within $\sim 20''$ of 3C 205, and of many other galaxies across that field, are consistent with 2–3 Gyr old ellipticals formed in a 1-Gyr burst. If these galaxies and the three even redder ones are all early-type galaxies at the quasar redshift, then we may be seeing a dispersion in the colors, metallicities, or ages of early-type cluster galaxies or their progenitors.

In the field of Q 1126+101, there are three dozen objects with $J-K_s>2.5$, a distinct excess compared to other fields, which themselves show an excess of such “ J -dropouts” compared with literature control fields. Several lines of argument suggest about half of these galaxies are most likely old and dusty (~ 2 Gyr, $E(B-V)\sim 0.75$) galaxies at the quasar redshifts with young (<0.1 Gyr) components comprising $\sim 1\%$ of their masses. The remaining J -dropouts are consistent with being at $z\gtrsim 2.5$, which places the 4000 Å break between J and K_s .

The possible presence of relatively old, dusty galaxies at the quasar redshifts coupled with the possible dispersion in early-type galaxy ages mentioned earlier suggests there may be considerable dispersion in the properties of cluster ellipticals at $z\sim 1.5$, in agreement with hierarchical clustering models (Kauffmann 1996). However, these candidate relatively old, dusty galaxies could also be younger systems with higher $E(B-V)$.

8. Conclusions

The major results of our study so far are:

- We find a significant excess of $K\gtrsim 19$ galaxies in the fields of 31 $z=1-2$ RLQs, on two spatial

scales (§2.1). One component is at $\theta < 40''$ from the quasars and is significant compared to the galaxy surface density at $\theta > 40''$ in the same fields. The other component appears roughly constant across the fields to $\theta \sim 100''$ from the quasars and is significant compared to the galaxy surface density seen in random-field surveys in the literature. The $\theta < 40''$ component may be produced by as few as $\sim 25\%$ of the $z > 1.4$ fields but the large-scale component is present in $\gtrsim 50\%$ of them.

- The $r-K$ color distributions of the excess galaxy populations are indistinguishable from each other and are significantly redder than the color distribution of the field population, consistent with the excess galaxies being predominantly at $z > 1$ (§3.1). However, there is a deficit of blue ($r-K \lesssim 3.5$) galaxies at $K=20-21$ which is difficult to understand as either real or spurious.
- The magnitudes and colors of the excess galaxies are consistent with a population of mostly early-type galaxies at the quasar redshifts, such as would be found in quasar host clusters or groups. There is no evidence that they are associated with intervening Mg II absorbers (§4.3).
- The average excess within $0.5h_{75}^{-1}$ Mpc ($\sim 65''$) of the quasars corresponds to Abell richness class $\sim 0 \pm 1$ compared to the galaxy surface density at $> 0.5h_{75}^{-1}$ Mpc from the quasars, where -1 denotes the richness of the field, and to Abell richness class $\sim 1.5 \pm 1.5$ compared to the galaxy surface density from the literature (§4). This assumes that the excess galaxies are all at the quasar redshifts. This suggests that on a large scale ($\gtrsim 0.75h_{75}^{-1}$ Mpc) RLQs at $z=1-2$ are located within clusters and/or large scale galaxy structures of Abell richness ~ 1.5 . On a smaller scale ($\lesssim 0.5h_{75}^{-1}$ Mpc) within those structures, RLQs can be located in unremarkable “field” environments or in groups or clusters of Abell richness ~ 0 . One uncertainty not taken into account when calculating richness measurements is the correspondence between individual galaxies at $z > 1$ and $z \sim 0$. A high merger rate at $z < 1-2$ would mean that individual galaxies at $z \sim 0$ were composed of several progenitors at $z > 1-2$, which could bias our richness measurements high. Spectroscopy and detailed comparison with numerical simulations are needed to resolve this uncertainty.
- The only significant correlations observed between environments and quasar properties is that the galaxy excess at $\theta < 40''$ seems to be stronger for the more radio-powerful and steeper-radio-spectrum RLQs (§2.2). The $\theta < 40''$ excess does not seem to depend on the presence of associated absorption. These dependences are based on only 31 RLQs (or fewer), but they at least illustrate trends which could be verified with larger datasets.
- By assuming the excess galaxies are at the quasar redshifts and fitting their K -band luminosity function, we find $-0.65_{-0.55}^{+0.41}$ magnitudes of luminosity evolution in M_K^* to $\bar{z}=1.67$ (§5). This is in contrast to the trends seen at $z > 1$ by Cowie *et al.* (1996) and Aragón-Salamanca *et al.* (1994), but plausibly in agreement with the work of Schade and collaborators (Schade 1996).
- For four fields with data in at least rJK_s , we find that the SEDs of most of the excess galaxies are consistent with them being 2–3 Gyr old early-type galaxies at the quasar redshifts of $z \sim 1.5$, but that there are galaxies whose SEDs cannot be fit by such simple models (§7). At least three objects in these four fields have SEDs consistent with being 4–5 Gyr old at $z \sim 1.5$, and at least a dozen others are consistent with ~ 2 Gyr old but dust-reddened galaxies at the quasar redshifts

(§7.4). Taken together, these potentially different galaxy types suggest that there is considerable dispersion in the properties of early-type cluster galaxies at $z \sim 1.5$, in agreement with hierarchical clustering models (Kauffmann 1996). However, these galaxies could also be younger systems with higher $E(B-V)$. Spectroscopic followup will be needed to confirm this suggestion. In particular, age determinations from deep spectra of the candidate 4–5 Gyr old galaxies offer the possibility of constraining the cosmological model by requiring a relatively old universe at large lookback times.

- There are also several dozen galaxies in the four fields with good J data (particularly in the Q 1126+101 field) whose SEDs are best explained either as background galaxies at $z \gtrsim 2.5$ or very dusty galaxies at $z = z_q$ (§7.3). Some of the $z \gtrsim 2.5$ candidates seem to be dusty, to have composite stellar populations, or both, and some may be already $\gtrsim 2$ Gyr old at $z \gtrsim 2.5$, again offering a possible constraint on cosmological models.

Without spectroscopic confirmation it is premature to draw firm conclusions about the implications of the existence of the excess galaxy population in these $z=1-2$ RLQ fields. Nonetheless, if we assume that the excess galaxies are predominantly at the quasar redshifts, we can draw some interesting conclusions which illustrate the value of spectroscopic followup.

The existence of galaxy excesses on two spatial scales, consistent with Abell richness $\sim 0 \pm 1$ clusters embedded in Abell richness $\sim 1.5 \pm 1.5$ structures if the excess galaxies are at the quasar redshifts, might lend support to hierarchical clustering models independent of Ω . This is because in such models clusters are built up by accretion of smaller clusters and groups over time. Galaxy structures embedded in larger structures such as we observe could occur during some phases of cluster formation in hierarchical clustering models.

This hierarchical clustering interpretation of the galaxy excesses on two spatial scales may tie in with RLQ host cluster observations at $z < 0.7$ (see §1 and the introduction to Paper 1). At such redshifts the clusters appear to be younger and less virialized than optically-selected clusters (Ellingson, Green & Yee 1991) and are of Abell richness 0–1, with a few of richness 2. At $z=1-2$ we also find that RLQs can be found in overdensities of Abell richness 0–1, but that these “near-field” overdensities are embedded in larger structures of Abell richness $\gtrsim 1$. It is an open question whether the most important factor affecting the evolution of RLQs in clusters is the absolute density of the environment, the density within 0.5 Mpc, or even conditions in the host galaxy and any galaxies interacting with it. However, despite the fact that an Abell richness 0 (sub)cluster observed at $z=1.5$ will evolve into a very different structure at $z=0$ than an Abell richness 0 cluster observed at $z=0.5$ will, we observe RLQs in Abell richness ~ 0 (within $0.5h_{75}^{-1}$ Mpc) clusters at both $z \sim 0.5$ and $z \sim 1.5$. This may imply that it is the properties of a RLQ’s environs within 0.5 Mpc which determine whether the environs are hospitable to RLQ formation and fueling; whether or not the Abell richness ~ 0 cluster is embedded in a larger structure or not may be immaterial. Alternatively, if clusters embedded in different large-scale environments show important differences in their formation histories, then the large-scale density of the RLQ’s environs would be what determines which clusters host RLQs. If this is the case then

the important result is that quasar host clusters at $z\sim 1.5$ are richer on large scales than at $z\sim 0.5$.

If we assume instead that the interpretation of Ellingson, Green & Yee (1991) is correct, i.e. that galaxy interactions are largely responsible for creating and fueling RLQs and that only dynamically young clusters are hospitable to RLQ, then one interpretation of our $z=1-2$ results would be that we are seeing dynamically young subclusters which will later virialize and/or merge with other galaxies or subclusters in the observed large-scale galaxy structures to form clusters as we know them today. The fact that RLQ host clusters at $z=1-2$ are not markedly richer on $0.5h_{75}^{-1}$ Mpc scales than those at $z<0.7$ is again consistent with hierarchical clustering models. In such models richer clusters do not undergo monolithic collapse at higher z , but instead form from mergers of subclusters at higher z .

The above speculations should be treated as such. Spectroscopic investigation of these fields and detailed comparison to numerical simulations is needed before we can begin to formulate a true model of the evolution of quasar environments to $z=2$. Nonetheless, if and when such confirmation is obtained, we feel that the above discussion outlines a reasonable framework for future thinking on this subject.

Among the followup research projects suggested by this work, two will be very important in confirming (or denying) and extending our results. First, larger areas ($>4' \times 4'$) around our sample need to be imaged to confirm the large-scale ($\theta\sim 100''$) galaxy excess around $z=1-2$ RLQs and to determine the true angular extent of this excess. Second, multislit optical and near-IR spectroscopy is needed to verify the existence of overdensities at the quasar redshifts, to determine velocity dispersions of any large-scale structures found, and to discriminate age, metallicity, and dust effects in the brightest candidate $z>1$ galaxies. Over the next decade IR spectrographs will begin to appear on 8-m class telescopes (e.g., the MMT 6.5m, LBT, and Keck) and perhaps the Next Generation Space Telescope. These instruments will enable spectroscopic identification of very red and faint galaxies and studies of their ages, metallicities, and dust reddenings. Ultimately, they may enable the fundamental plane of elliptical galaxies and its evolution to be studied to $z=1-2$ and beyond using galaxies from this and other work.

This work was part of a Ph.D. thesis at the University of Arizona. PBH acknowledges support from an NSF Graduate Fellowship and from NASA. We thank M. Dickinson and R. Elston and their collaborators for use of data prior to publication, all authors who have made all or part of their K band imaging datasets publicly available for ourselves and others to use, and the referee for interesting and helpful comments. This research has made use of observations made at the Kitt Peak National Observatory, National Optical Astronomy Observatories, which is operated by the Association of Universities for Research in Astronomy (AURA), Inc., under contract to the National Science Foundation, and at the Infra-Red Telescope Facility, which is operated by the University of Hawaii under contract to the National Aeronautics and Space Administration; the NASA/IPAC Extragalactic Database (NED), operated by the Jet Propulsion Laboratory, California Institute of Technology, under contract to NASA; and data from operations made with

the NASA/ESA Hubble Space Telescope, obtained from the data archive at the Space Telescope Science Institute, which is operated by AURA, Inc., under NASA contract NAS 5-26555.

A. Literature Control-Field Data

Since our own control fields cover far less area than our RLQ fields, it is advantageous to have as much additional control field data as possible, preferably with data in r and K_s . Of the datasets available in the literature, however, few utilize those specific filters. For purposes of comparing color-magnitude diagrams, it is acceptable to use data in various optical filters to estimate r magnitudes, since the uncertainties in predicting $r-K_s$ from $I-K$ (e.g.) for faint galaxies are smaller than the binning size of $0^m.5$ we will typically use in our comparisons. To estimate galaxy colors in one optical filter set from another, we use the galaxy colors for morphological types E through Im which have been computed by Frei & Gunn (1994; FG94) from $z=0-0.6$ using the SEDs of Coleman, Wu & Weedman (1980), and by Fukugita, Shimasaku, & Ichikawa (1995; FSI95) from $z=0-0.8$ using the spectral atlas of Kennicutt (1992). Specifically, we use Tables 2–6 of FG94 and Tables 3–9 of FSI95 where both references give consistent first-order color-color conversion results (after accounting for different zeropoints in the two references, cf. Appendix A of Paper 1) and FSI95 alone where they do not.

At $K_s < 20$, for $r-K_s$ comparisons we use primarily our two control fields (18.78 arcmin², R_C and K_s), the McLeod *et al.* (1995) Her-1 field (10.56 arcmin², Tyson R_T and K_s), the HDS (Cowie *et al.* 1994) SSA13, 17, and 22 fields (5.33 arcmin², $U' B V I_C$ and K), and preliminary data (25 arcmin², R_C and K_s) from the SA57 field of the 100 arcmin² $BRIzJK$ KPNO 4m+IRIM survey of Elston, Eisenhardt, & Stanford (1998; EES98), kindly provided by R. Elston. At $K_s > 20$, we use the Djorgovski *et al.* (1995) Hercules field (0.44 arcmin², r and K_s), the Moustakas *et al.* (1997) Fields I and II (2.88 arcmin², $V I K$), and the preliminary KPNO 4m+IRIM catalogs of the Hubble Deep Field (HDF-IRIM; 7.40 arcmin², $F606W, F814W, JHK$), kindly provided by M. Dickinson (cf. Dickinson *et al.* 1998). Conservative uncertainties of $\pm 0^m.1$ were assigned to magnitudes, and $\pm 0^m.15$ to colors, where none were given. We only removed objects classified stellar by the various authors, who used varying criteria including morphologies and colors (cf. Saracco *et al.* 1997). Stellar contamination is not a large effect at faint magnitudes, but should be kept in mind nonetheless, particularly for the HDF-IRIM and EES98 datasets which still include stars.

We estimated the r and i magnitudes of the McLeod objects from their R_T and I_T magnitudes (Gullixson *et al.* 1995) using relations derived from FSI95 and our adopted zeropoints (see Appendix A of Paper 1 and Appendix A of this paper):

$$r = R_T + 0.367 - 0.048 \times (R_T - I_T) \tag{A1}$$

$$i = I_T + 0.710 + 0.045 \times (R_T - I_T) \tag{A2}$$

We estimated the r magnitudes of the EES98 objects from their R_C magnitudes using a relation

derived from both FG94 and FSI95:

$$r = R_C + 0.322 \tag{A3}$$

This is the same relation used for our own control fields and the Q 2230+114 field, and the color term is negligibly small. We estimated the r magnitudes of the Moustakas and HDS objects from their V and I_C magnitudes using a relation derived from both FG94 and FSI95:

$$r = I_C + 0.447 + 0.452 \times (V - I_C). \tag{A4}$$

The 1σ scatter around this fit is the largest of all our fits, but is still $\pm 0^m1$ or less at $z \lesssim 1$. (The published V and I magnitudes for Field II of Moustakas *et al.* are in error and should be adjusted by -1^m6 and $+1^m6$ respectively.) For the Dickinson *et al.* (1998) data, we convert the HDF $F606W$ and $F814W$ AB magnitudes to Vega-based magnitudes which we dub V_{606} and I_{814} using $V_{606} = F606W - 0.116$ and $I_{814} = F814W - 0.439$ (Williams *et al.* 1996). We then convert to V and I_C using $V = V_{606} + 0.37(V_{606} - I_{814})$ and $I_C = I_{814} - 0.10(V_{606} - I_{814})$, which are first-order approximations derived from Tables 10 and 7 of Holtzman *et al.* (1995). Finally, we estimate r from V and I_C as for the Moustakas data above.

Control field J band data were taken directly from the McLeod *et al.* (1995) SA57SO field, the EES98 SA57 field, and the HDF-IRIM data (Dickinson *et al.* 1998).

We use several different combinations of these datasets in our work. We exclude the Soifer *et al.* (1994) data since those fields were targeted around high redshift objects and are thus not the random fields we desire as control fields. By “published control fields” we refer to all datasets mentioned above, except the HDF-IRIM and EES98 datasets, plus the bright-end data of Glazebrook *et al.* (1994) and the HMWS and HMWS (Gardner 1995a; Gardner 1995b). By “opt-IR control fields” we refer to all datasets from which we generated $r-K_s$ colors, including our own. This includes only parts of some datasets: all but the HDS SSA4 field of Cowie *et al.* (1994), just the Hercules field of Djorgovski *et al.* (1995), just the Her-1 field of McLeod *et al.* (1995), and just the SA57 field of EES98.

To check that our conversions of the various literature colors to $r-K$ colors are accurate, we compare $r-K$ distributions in Figure 10. The dotted lines are all opt-IR control fields except our own, and the solid lines are our own control fields and those of Djorgovski *et al.* (1995), which are the only fields with data originally taken in r (or R) and K_s . The uncertainties are large, but there are no significant differences between the actual and converted $r-K$ distributions at any $K=17-21$, i.e. between our control field data and that from the literature, given the deeper limits of many of the opt-IR control fields.

REFERENCES

- Abell, G. O. 1958, ApJS, 3, 211
 Aldcroft, T., Bechtold, J., and Elvis, M. 1994, ApJS, 93, 1

- Anderson, S. F., Weymann, R. J., Foltz, C. B., and Chaffee, F. H. 1987, *AJ*, 94, 278
- Aragón-Salamanca, A., Ellis, R., Couch, W., and Carter, D. 1993, *MNRAS*, 262, 764 (AS93)
- Aragón-Salamanca, A., Ellis, R. S., Schwartzberg, J.-M., and Bergeron, J. A. 1994, *ApJ*, 421, 27
- Aragón-Salamanca, A., Ellis, R. S., and O’Brien, K. S. 1996, *MNRAS*, 281, 945
- Aragón-Salamanca, A., Baugh, C. M., and Kauffmann, G. 1997, to appear in “The Young Universe,” eds. S. D’Odorico, A. Fontana and E. Giallongo (ASP: San Francisco) (astro-ph/9711146)
- Bahcall, N. A. 1981, *ApJ*, 247, 787
- Bahcall, N. A., Fan, X., and Cen, R. 1997, *ApJ*, 485, L53
- Barger, A. J., Aragón-Salamanca, A., Ellis, R. S., Couch, W. J., Smail, I., and Sharples, R. M. 1995, *MNRAS*, 279, 1
- Barrientos, L. F., Schade, D., and Lopez-Cruz, O. 1996, *ApJ*, 460, L89
- Baugh, C. M., Gardner, J. P., Frenk, C. S., and Sharples, R. M. 1996, *MNRAS*, 283, L15
- Bechtold, J., and Ellingson, E. 1992, *ApJ*, 396, 20
- Bechtold, J., Elston, R., Yee, H. K. C., Ellingson, E., and Cutri, R. M. 1998, to appear in “The Young Universe: Galaxy Formation and Evolution at Intermediate and High Redshift”, eds. S. d’Odorico, A. Fontana, & E. Giallongo (ASP: San Francisco) (astro-ph/9802230)
- Bender, R., Ziegler, B., and Bruzual A., G. 1996, *ApJ*, 463, 51
- Benítez, N., Martínez-González, E., and Martín-Mirones, J. M. 1997, *A&A*, 321, L1
- Bergeron, J., and Boisse, P. 1991, *A&A*, 243, 344
- Bershady, M. A., Lowenthal, J. D., and Koo, D. C. 1998, *ApJ*, in press (astro-ph/9804093)
- Best, P. N., Longair, M. S., and Röttgering. H. J. A. 1998, *MNRAS*, 295, 549 (astro-ph/9709195)
- Best, P. N., Longair, M. S., and Röttgering. H. J. A. 1997, to appear in proceedings of “The Most Distant Radio Galaxies” (astro-ph/9711010)
- Bica, E., Alloin, D., Bonatto, C., Pastoriza, M. G., Jablonka, P., Schmidt, A., and Schmitt, H. R. 1996, in “A Data Base for Galaxy Evolution Modeling,” eds. C. Leitherer *et al.*, *PASP*, 108, 996
- Bithell, M., and Rees, M. J. 1990, *MNRAS*, 242, 570
- Brinchmann, J., *et al.* 1998, *ApJ*, 499, 112 (astro-ph/9712060)
- Bruzual A., G., and Charlot, S. 1993, *ApJ*, 405, 538
- Bruzual A., G., and Charlot, S. 1996, in “A Data Base for Galaxy Evolution Modeling,” eds. C. Leitherer *et al.*, *PASP*, 108, 996
- Bruzual A., G., and Magris C., G. 1997, to appear in “The Hubble Deep Field,” eds. M. Livio, S. M. Fall, and P. Madau (STScI: Baltimore) (astro-ph/9707154)
- Bunker, A. J., Warren, S. J., Hewett, P. C., and Clements, D. L. 1995, *MNRAS*, 273, 513
- Burrows, A., Marley, M., Hubbard, W. B., Lunine, J. I., Guillot, T., Saumon, D., Freedman, R., Sudarsky, D., and Sharp, C. 1997, *ApJ*, 491, 856
- Butcher, H. R. and Oemler, A. 1984, *ApJ*, 285, 426
- Calzetti, D. 1997, to appear in “The Ultraviolet Universe at Low and High Redshift,” eds. W. H. Waller, M. N. Fanelli, and A. C. Danks (AIP: New York) (astro-ph/9706121)
- Carlberg, R. G., Cowie, L. L., Songaila, A., and Hu, E. M. 1997, *ApJ*, 484, 538
- Chaboyer, B., Demarque, P., Kernan, P. J., and Krauss, L. M. 1998, *ApJ*, 494, 96 (astro-ph/9706128)
- Charlot, S., Ferrari, F., Mathews, G. J., and Silk, J. 1993, *ApJ*, 419, L57

- Charlot, S., Worthey, G., and Bressan, A. 1996, *ApJ*, 457, 625
- Cimatti, A., Bianchi, S., Ferrara, A., and Giovanardi, C. 1997, *MNRAS*, 290, L43
- Cowie, L. L., Gardner, J. P., Hu, E. M., Songaila, A., Hodapp, K.-W., and Wainscoat, R. J. 1994, *ApJ*, 434, 114
- Cowie, L. L. 1996, in “HST and the High Redshift Universe,” eds. N. Tanvir, A. Aragón-Salamanca, and J. V. Wall (World Scientific: Singapore)
- Cowie, L. L., Songaila, A., Hu, E. M., and Cohen, J. G. 1997, *AJ*, 112, 839
- Crawford, C. S., and Fabian, A. C. 1996, *MNRAS*, 281, L5
- Crawford, C. S., and Fabian, A. C. 1996, *MNRAS*, 282, 1483
- Deltorn, J. M., Le Fèvre, O., Crampton, D., and Dickinson, M. 1996, in “The Early Universe with the VLT,” ed. J. Bergeron (Springer-Verlag: Berlin)
- Deltorn, J. M., Le Fèvre, O., Crampton, D., and Dickinson, M. 1997, *ApJ*, 483, L21 (astro-ph/9704086)
- De Vaucouleurs, G. 1975, *ApJ*, 202, 319
- Dickinson, M. 1995, in “Fresh Views on Elliptical Galaxies,” ed. A. Buzzoni, A. Renzini, and A. Serrano (ASP: San Francisco) (astro-ph/9507064), 283
- Dickinson, M. 1996a, in “HST and the High Redshift Universe,” eds. N. Tanvir, A. Aragón-Salamanca, and J. V. Wall (World Scientific: Singapore) (astro-ph/9612178)
- Dickinson, M. 1996b, in “The Early Universe with the VLT,” ed. J. Bergeron (Springer-Verlag: Berlin) (astro-ph/9612177)
- Dickinson *et al.* 1997, to appear in “Galaxy Scaling Relations: Origins, Evolution and Applications,” ed. L. da Costa (Springer-Verlag: Berlin) (astro-ph/9703035)
- Dickinson *et al.* 1998, in preparation
- Djorgovski, S., Soifer, B. T., Pahre, M. A., Larkin, J. E., Smith, J. D., Neugebauer, G., Smail, I., Matthews, K., Hogg, D. W., Blandford, R. D., Cohen, J., Harrison, W., and Nelson, J. 1995, *ApJ*, 438, L13
- Donahue, M., Gioia, I. M., Luppino, G., Hughes, J. P., and Stocke, J. T. 1998, *ApJ*, in press (astro-ph/9707010)
- Dressler, A. 1980, *ApJ*, 236, 351
- Dunlop, J., Peacock, J., Spinrad, H., Dey, A., Jimenez, R., Stern, D., and Windhorst, R. 1996, *Nature*, 381, 581
- Eales, S., Rawlings, S., Dickinson, M., Spinrad, H., Hill, G. J., and Lacy, M. 1993, *ApJ*, 409, 578
- Eddington, A. S., 1913, *MNRAS*, 73, 359
- Ellingson, E., Green, R. F., and Yee, H. K. C. 1991, *ApJ*, 378, 475 (EGY91)
- Ellingson, E., Yee, H. K. C., and Green, R. F. 1991, *ApJ*, 371, 49
- Ellingson, E., and Yee, H. K. C. 1994, *ApJS*, 92, 33
- Ellingson, E., Yee, H. K. C., Bechtold, J., and Dobrzycki, A. 1994, *AJ*, 107, 1219
- Elston, R. 1994, in “Infrared Astronomy with Arrays,” ed. I. McLean (Kluwer: Dordrecht), 33
- Elston, R., Eisenhardt, P., and Stanford, S. A. 1998, in preparation (EES98)
- Engelbracht, C. W. 1997, Ph.D. Thesis, University of Arizona
- Fioc, M., and Rocca-Volmerange, B. 1997, *A&A*, 326, 950 (astro-ph/9707017)
- Fukugita, M., Shimasaku, K., and Ichikawa, T. 1995, *PASP*, 107, 945
- Foltz, C. B., Weymann, R. J., Peterson, B. M., Sun, L., Malkan, M. A., and Chaffee, F. 1986, *ApJ*, 307, 504
- Foltz, C. B., Chaffee, F., Weymann, R., and Anderson, S. 1988, in “Quasar Absorption Lines: Probing the Universe” (Cambridge: Cambridge), 53

- Fouque, P., Bertin, E., Dec, P. A., and Chevallier, L. 1997, in “The Impact of Large Scale Near-IR Sky Surveys,” eds. F. Garzón, N. Epchtein, A. Omont, B. Burton, and P. Persi (Kluwer: Dordrecht)
- Francis, P. J., Woodgate, B. E., and Danks, A. C. 1997, *ApJ*, 482, L25
- Frei, Z., and Gunn, J. E. 1994, *AJ*, 108, 1476
- Gardner, J. P. 1995a, *ApJS*, 98, 441
- Gardner, J. P. 1995b, *ApJ*, 452, 538
- Gardner, J. P., Sharples, R. M., Carrasco, B. E., and Frenk, C. S. 1996, *MNRAS*, 282, L1
- Gardner, J. P., Sharples, R. M., Frenk, C. S., and Carrasco B. E. 1997, *ApJ*, 480, L99
- Gehrels, N. 1986, *ApJ*, 303, 336
- Glazebrook, K., Peacock, J. A., Collins, C. A., and Miller, L. 1994, *MNRAS*, 266, 65
- Glazebrook, K., Peacock, J. A., Miller, L., and Collins, C. A. 1995, *MNRAS*, 275, 169
- Graham, J. P., and Dey, A. 1996, *ApJ*, 471, 720
- Gullixson, C. A., Boeshaar, P. C., Tyson, J. A., and Seitzer, P. 1995, *ApJS*, 99, 281
- Haehnelt, M. G., Steinmetz, M., and Rauch, M. 1996, *ApJ*, 465, L95
- Hall, P. B., Ellingson, E., Green, R. F., and Yee, H. K. C. 1995, *AJ*, 110, 513
- Hall, P. B., Ellingson, E., and Green, R. F. 1997, *AJ*, 113, 1179
- Hall, P. B. 1998, Ph.D. Thesis, University of Arizona
- Hall, P. B., Cohen, M., and Green, R. F. 1998, *ApJS*, in press (Paper 1)
- Hardy, E., and Delisle, S. 1996, in “A Data Base for Galaxy Evolution Modeling,” eds. C. Leitherer *et al.*, *PASP*, 108, 996
- Heap, S. R., *et al.* 1998, *ApJ*, 492, L131 (astro-ph/9711074)
- Hill, G., and Lilly, S. 1991, *ApJ*, 367, 1
- Hogg, D. W., and Turner, E. L. 1997, *PASP*, in press (astro-ph/9711154)
- Holtzman, J. A., Burrows, C. J., Casertano, S., Hester, J. J., Trauger, J. T., Watson, A. M. and Worthey, G. 1995, *PASP*, 107, 1065
- Howarth, I. D. 1983, *MNRAS*, 203, 301
- Hu, E. M., and Ridgway, S. E. 1994, *AJ*, 107, 1303
- Hudson, M. J., Gwyn, S. D. J., Dahle, H., and Kaiser, N. 1997, *ApJ*, in press (astro-ph/9711341)
- Hutchings, J. B. 1990, *PASP*, 102, 431
- Kauffmann, G., and Charlot, S. 1998, *MNRAS*, 294, 705 (astro-ph/9704148)
- Kauffmann, G. 1996, *MNRAS*, 281, 487 (astro-ph/9502096)
- Kennicutt, R. C. 1992, *ApJS*, 79, 255
- Kronberg, P. P., Dyer, C. C., and Röser, H.-J. 1996, *ApJ*, 472, 115
- Lebofsky, M. J., and Eisenhardt, P. R. M. 1986, *ApJ*, 300, 151
- Lejeune, T., Buser, R., and Cuisinier F. 1996, in “A Data Base for Galaxy Evolution Modeling,” eds. C. Leitherer *et al.*, *PASP*, 108, 996
- Lidman, C. E., and Peterson, B. A. 1996, *AJ*, 112, 2454
- Lin, H., Kirschner, R. P., Schectman, S. A., Landy, S. D., Oemler, A., Tucker, D. L., and Schechter, P. L. 1996, *ApJ*, 471, 617

- Lilly, S. J., *et al.* 1997, submitted (astro-ph/9712061)
- Lonsdale, C. J., and Barthel, P. D. 1986, *AJ*, 92, 12
- Lonsdale, C. J., and Barthel, P. D. 1988, in “The impact of VLBI on astrophysics and geophysics,” eds. M. J. Reid and J. M. Moran, 135
- Lonsdale, C. J., and Barthel, P. D. 1998, *AJ*, 115, 895
- Lubin, L. M. 1996, *AJ*, 112, 23
- Magris C., G., and Bruzual A., G. 1997, *ApJ*, 417, 102
- Mannucci, F., Thompson, D., Beckwith, S. V. W., and Williger, G. M. 1998, *ApJ*, in press (astro-ph/9805103)
- McLeod, B. A. 1994, Ph.D. Thesis, University of Arizona
- McLeod, B. A., Bernstein, G. M., Rieke, M. J., Tollestrup, E. V., and Fazio, G. G. 1995, *ApJS*, 96, 117
- Mobasher, B., Sharples, R. M., and Ellis, R. S. 1993, *MNRAS*, 263, 560
- Morris, S. L., Weymann, R. J., Foltz, C. B., Turnshek, D. A., Schectman, S., Price, C., and Boroson, T. A. 1986, *ApJ*, 310, 40
- Morris, S. L., Weymann, R. J., Dressler, A., McCarthy, P. J., Smith, B. A., Terrile, R. J., Giovanelli, R., and Irwin, M. 1993, *ApJ*, 419, 524
- Moustakas, L. A., Davis, M., Graham, J. R., Silk, J., Peterson, B., and Yoshii, Y. 1997, *ApJ*, 475, 445
- Pahre, M., Djorgovski, S., and de Carvalho, R. 1996, *ApJ*, 456, 79
- Poggianti, B. M. 1997, *A&AS*, 122, 399
- Postman, M., and Lauer, T. R. 1995, *ApJ*, 440, 28
- Postman, M., Lubin, L. M., Gunn, J. E., Oke, J. B., Hoessel, J. G., Schneider, D. P., and Christensen, J. A. 1996, *AJ*, 111, 615
- Prestage, R. M., and Peacock, J. A. 1988, *MNRAS*, 230, 131
- Rakos, K. D., and Schombert, J. M. 1995, *ApJ*, 439, 47
- Rauch, M., Haehnelt, M. G., and Steinmetz, M. 1997, *ApJ*, 481, 601
- Richstone, D., Loeb, A., and Turner, E. L. 1992, *ApJ*, 393, 477
- Ridgway, S., and Stockton, A. 1997, *AJ*, 114, 511
- Roche, N., Eales, S., and Hippelein, H. 1997, *MNRAS*, submitted (astro-ph/9711068)
- Roche, N., Eales, S., and Rawlings, R. 1997, *MNRAS*, submitted (astro-ph/9707100)
- Ruiz, M. T., Leggett, S. K., and Allard, F. 1997, *ApJ*, 491, L107
- Saracco, P., Iovino, A., Garilli, B., Maccagni, D., and Chincarini, G. 1997, *AJ*, 114, 887 (astro-ph/9706055)
- Sargent, W. L. W., Boksenberg, A., and Steidel, C. C. 1988, *ApJS*68, 539
- Sawicki, M., Lin, H., and Yee, H. K. C. 1997, *AJ*, 113, 1
- Sawicki, M., and Yee, H. K. C. 1998, *AJ*, 115, 1329 (astro-ph/9712216)
- Schade, D., Lilly, S. J., Crampton, D., Hammer, F., Le Fèvre, O., and Tresse, L. 1995, *ApJ*, 451, L1
- Schade, D., Lopez-Cruz, O., and Barrientos, L. F. 1997, *ApJ*, 477, L17
- Schade, D. 1996, in “HST and the High Redshift Universe,” eds. N. Tanvir, A. Aragón-Salamanca, and J. V. Wall (World Scientific: Singapore)
- Schechter, P. 1976, *ApJ*, 203, 297
- Schneider, P., van Waerbeke, L., Mellier, Y., Jain, B., Seitz, S., and Fort, B. 1997, *A&A*, 333, 767 (astro-ph//9705122)

- Seaton, M. J. 1979, MNRAS, 187, 73P
- Seldner, M., and Peebles, P. J. E. 1978, ApJ, 225, 7
- Shaver, P. A., Wall, J. V., Kellermann, K. I., Jackson, C. A., and Hawkins, M. R. S. 1996, Nature, 384, 439
- Skrutskie, M. F. *et al.* 1997, in “The Impact of Large Scale Near-IR Sky Surveys,” eds. F. Garzón, N. Epchtein, A. Omont, B. Burton, and P. Persi (Kluwer: Dordrecht)
- Smail, I., and Dickinson, M. 1995, ApJ, 455, L99
- Small, T. A., Ma, C.-P., Sargent, W. L. W., and Hamilton, D. 1998, ApJ, 492, 45 (astro-ph/9708153)
- Soifer, B. T., *et al.* 1994, ApJ, 420, L1
- Spinrad, H., Dey, A., Stern, D., Dunlop, J., Peacock, J., Jimenez, R., and Windhorst, R. 1997, ApJ, 484, 581
- Stanford, S. A., Eisenhardt, P. R. M., and Dickinson M. 1998, ApJ, 492, 461 (astro-ph/9708037)
- Stanford, S. A., Elston, R., Eisenhardt, P. R. M., Spinrad, H., Stern, D., and Dey, A. 1997, AJ, 114, 2232 (astro-ph/9709057)
- Steidel, C. C., and Dickinson, M. 1994, in “Wide Field Spectroscopy and the Distant Universe,” eds. S. J. Maddox and A. Aragón-Salamanca (World Scientific: Singapore)
- Steidel, C. C., Dickinson, M., and Persson, S. E. 1994, ApJ, 437, L75
- Steidel, C. C., Giavalisco, M., Pettini, M., Dickinson, M., and Adelberger, K. L. 1996, ApJ, 462, L17
- Steidel, C. C., Adelberger, K. L., Dickinson, M., Giavalisco, M., Pettini, M., and Kellogg, M. 1998, ApJ, 492, 428 (astro-ph/9708125)
- Steidel, C. C., Adelberger, K. L., Giavalisco, M., Dickinson, M., Pettini, M., and Kellogg, M. 1998, to appear in “The Young Universe,” eds. S. D’Odorico, A. Fontana and E. Giallongo (ASP: San Francisco) (astro-ph/9804237)
- Steinmetz, M. 1997, to appear in “Structure and Evolution of the IGM From QSO Absorption Line Systems”, eds. P. Petitjean and S. Charlot (Nouvelles Frontières: Paris) (astro-ph/9709260)
- Teplitz, H., Malkan, M., and McLean, I. 1998, ApJ, in press (astro-ph/9805157)
- Thuan, T. X., and Puschell, J. J. 1989, ApJ, 346, 34
- van Dokkum, P., and Franx, M. 1996, MNRAS, 281, 985
- Williams, R. E., *et al.* 1996, AJ, 112, 1335
- Wills, B. J., Thompson, K. L., Han, M., Netzer, H., Wills, D., Baldwin, J. A., Ferland, G. J., Browne, I. W. A., and Brotherton, M. S. 1995, ApJ, 447, 139
- Worthey, G. 1994, ApJS, 95, 107
- Yee, H. K. C., and Ellingson, E., 1993, ApJ, 411, 43 (YE93)
- Yee, H. K. C., and Green, R. F. 1984, ApJ, 280, 79
- Yee, H. K. C., and Green, R. F. 1987, ApJ, 319, 28 (YG87)
- Zepf, S. E. 1997, Nature, 390, 377 (astro-ph/9711355)

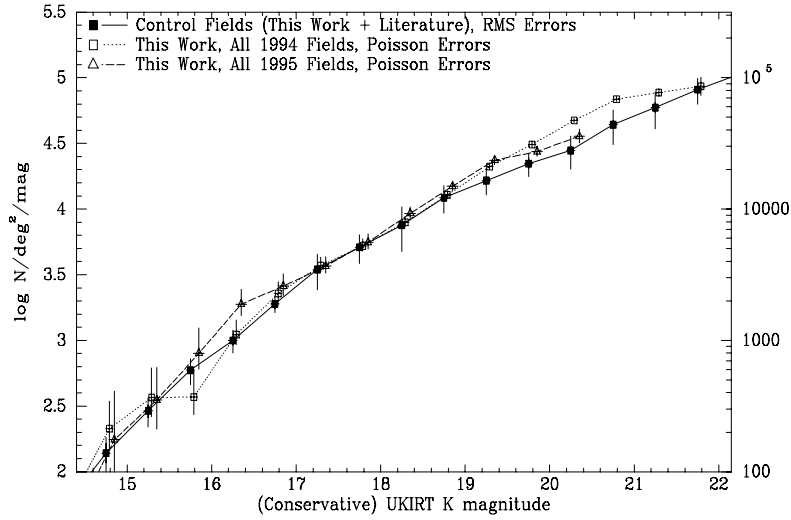


Fig. 1.— The conservative K_{UKIRT} $N(m)$ relations for our 1994 and 1995 KPNO 4m run data are plotted as dotted and dashed lines respectively. The area-weighted average of our conservative-magnitude control fields and all published random-field imaging surveys (corrected to K_{UKIRT}) is plotted as the solid line. RMS uncertainties are plotted for the $N(m)$ values and formal uncertainties for the magnitude bin centers.

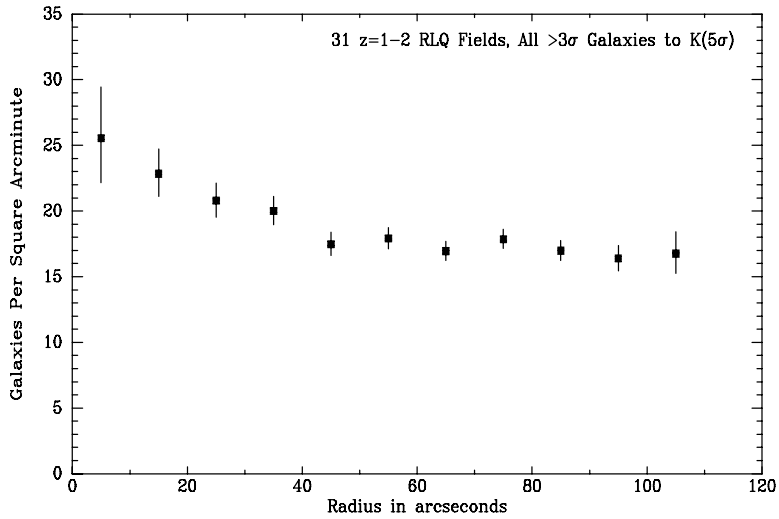


Fig. 2.— Radial distribution of galaxies relative to the quasars. All galaxies detected at $\geq 3\sigma$ down to the average 5σ magnitude limit in each field are included. Error bars are calculated for the number of objects in each bin as per Gehrels (1986). The large uncertainties are from small number statistics: at small radii the bin area is small, and at large radii only part of the full annulus is imaged, so the number of galaxies detected is small in both cases.

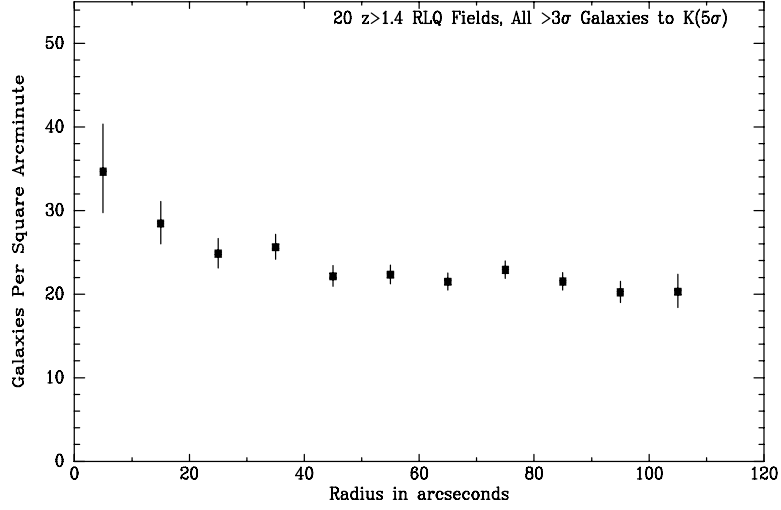


Fig. 3.— Radial distribution of galaxies in the $z > 1.4$ fields. All galaxies detected at $\geq 3\sigma$ down to the average 5σ magnitude limit in each field are included.

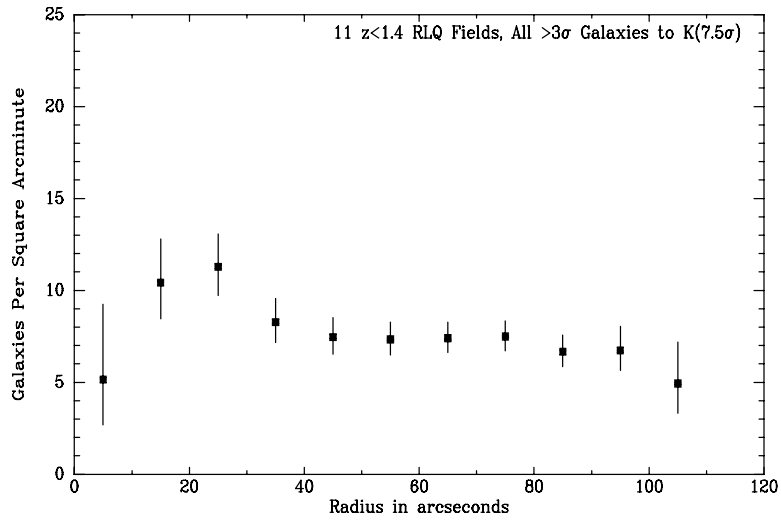


Fig. 4.— Radial distribution of galaxies in the $z < 1.4$ fields. All galaxies detected at $\geq 3\sigma$ down to the average 7.5σ magnitude limit in each field are included.

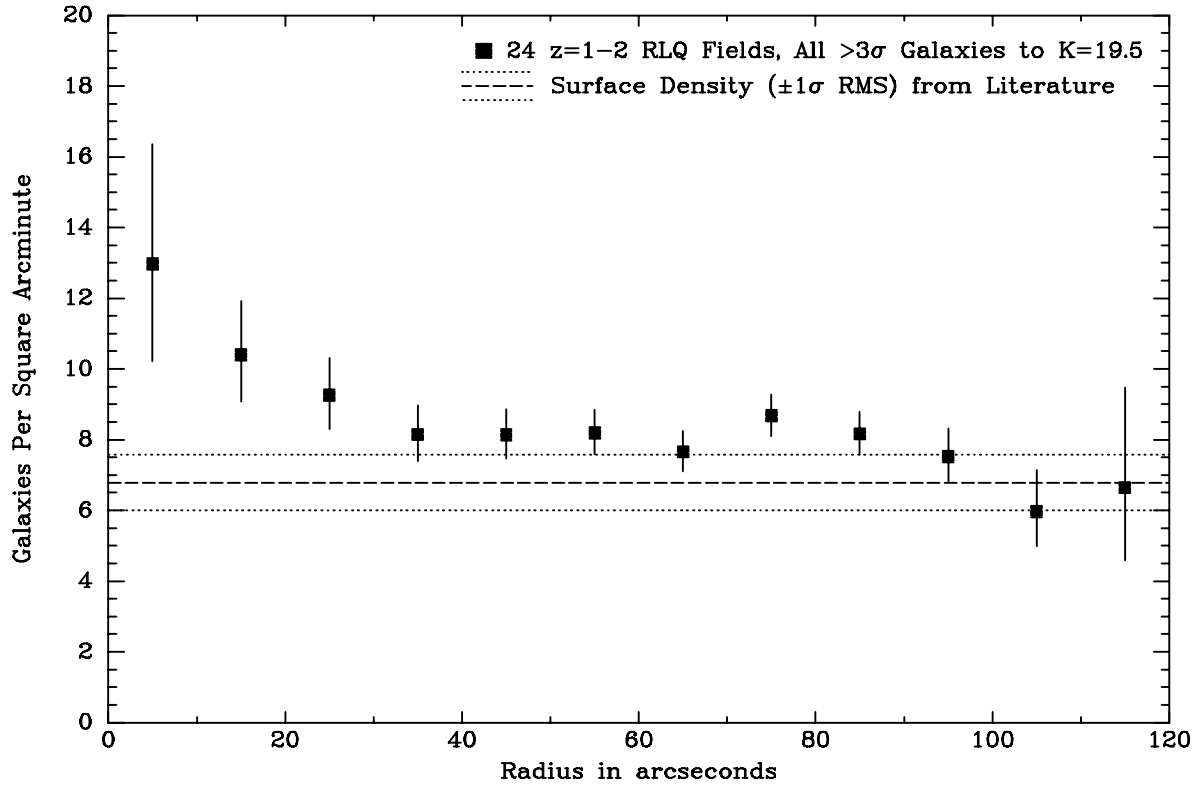


Fig. 5.— Radial distribution of galaxies relative to the quasars in all fields which reach at least $K=19.5$. All galaxies detected at $\geq 3\sigma$ down to the average 5σ magnitude limit in each field are included.

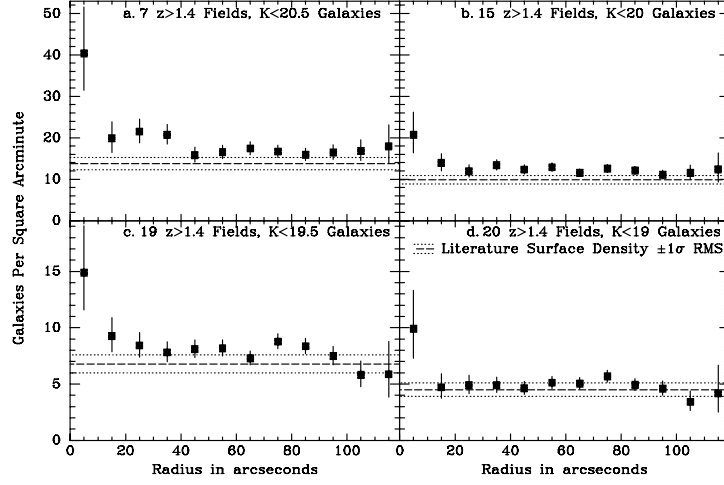


Fig. 6.— Radial distribution of galaxies in the $z > 1.4$ RLQ fields. Dashed line in both figures is the surface density from the average published literature counts, and dotted lines are the $\pm 1\sigma$ RMS uncertainties. a. All galaxies detected at $\geq 3\sigma$ down to $K_{UKIRT}=20.5$ in the 7 $z > 1.4$ RLQ fields with 5σ limits that deep. b. All galaxies detected at $\geq 3\sigma$ down to $K_{UKIRT}=20$ in the 15 $z > 1.4$ RLQ fields with 5σ limits that deep. c. All galaxies detected at $\geq 3\sigma$ down to $K_{UKIRT}=19.5$ in the 19 $z > 1.4$ RLQ fields with 5σ limits that deep. d. All galaxies detected at $\geq 3\sigma$ down to $K_{UKIRT}=19$ in all 20 $z > 1.4$ RLQ fields.

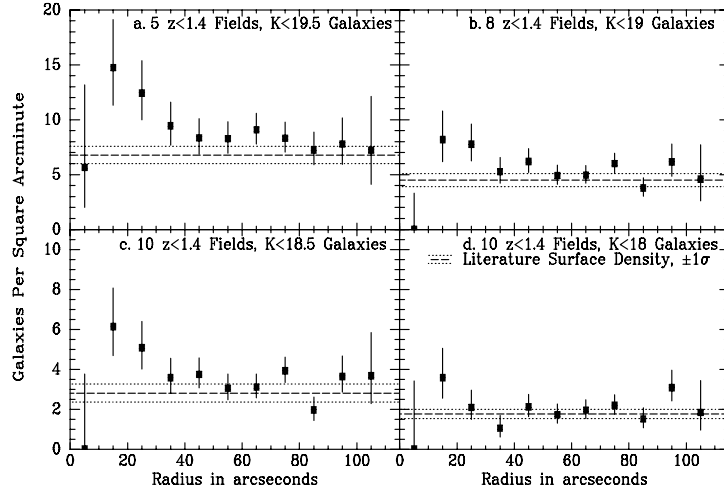


Fig. 7.— Radial distribution of galaxies in the $z < 1.4$ RLQ fields. Dashed line in both figures is the surface density from the average published literature counts, and dotted lines are the $\pm 1\sigma$ RMS uncertainties. a. All galaxies detected at $\geq 3\sigma$ down to $K_{UKIRT}=19.5$ in the 5 fields with 5σ limits that deep. b. All galaxies detected at $\geq 3\sigma$ down to $K_{UKIRT}=19$ in the 8 fields with 5σ limits that deep. c. All galaxies detected at $\geq 3\sigma$ down to $K_{UKIRT}=18.5$ in the 10 $z < 1.4$ RLQ Fields fields with 5σ limits that deep. d. All galaxies detected at $\geq 3\sigma$ down to $K_{UKIRT}=18$ in all 11 fields.

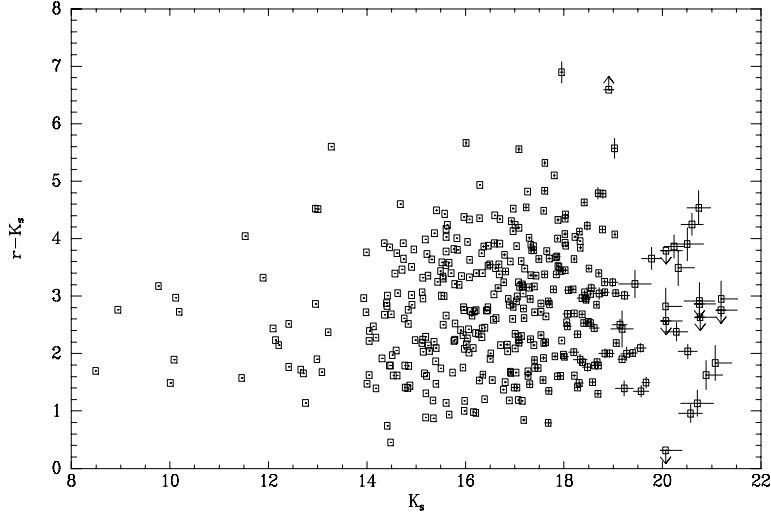


Fig. 8.— Morphologically identified stars’ isophotal $r-K_s$ colors vs. total K_s magnitudes. Error bars are 1σ photon noise only. Faint objects with only rightward error bars on their K_s magnitudes have total magnitude detections of $<3\sigma$, but may have isophotal magnitude detections of $>3\sigma$. All RLQ fields are plotted except Q 1508–055 (no r data) and Q 2230+114 (nonphotometric R_C data). The 31 remaining fields cover 219.2 arcmin^2 and contain 380 stars detected at $\geq 3\sigma$ in r or K_s .

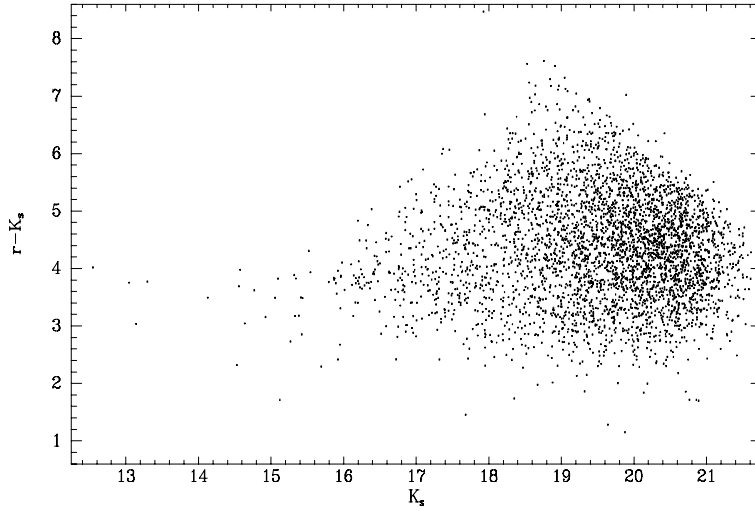


Fig. 9.— Galaxy $r-K_s$ colors vs. K_s magnitude. All RLQ fields are plotted except Q 1508–055 (no r data), Q 2230+114 (nonphotometric R_C data), and Q 0736–063 (uncertain stellar contamination). The 30 remaining fields cover 213.7 arcmin^2 and contain 3886 galaxies detected at $\geq 3\sigma$ in r or K_s and with K_s brighter than the average 5σ limits, all of which are plotted here. Note the reddest object at $K_s \sim 18$, $r-K_s \gtrsim 8.4$ (3σ lower limit).

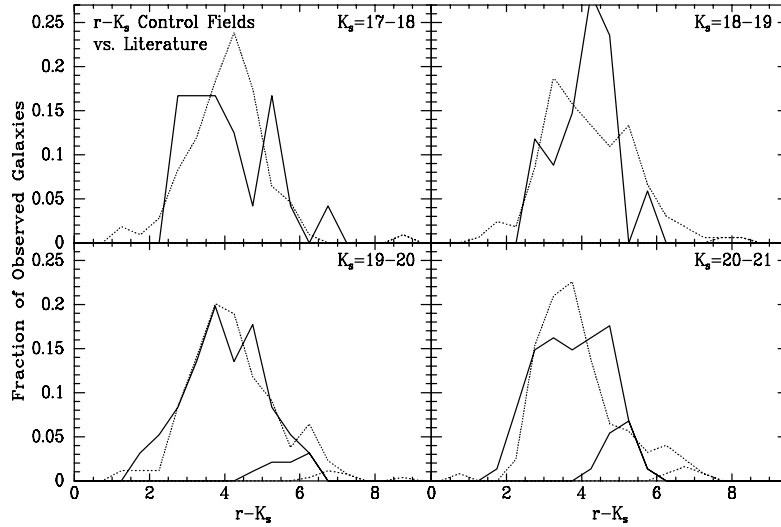


Fig. 10.— Comparison of K_s -selected galaxy $r-K_s$ colors between fields with actual r (or R) and K data (solid lines) and literature control fields with r and K data synthesized from magnitudes in other filters (dotted lines). Smaller histograms are galaxies with lower or upper limits to their colors. Each histogram has been separated normalized to unity sum. The K_s magnitude range is given in each panel.

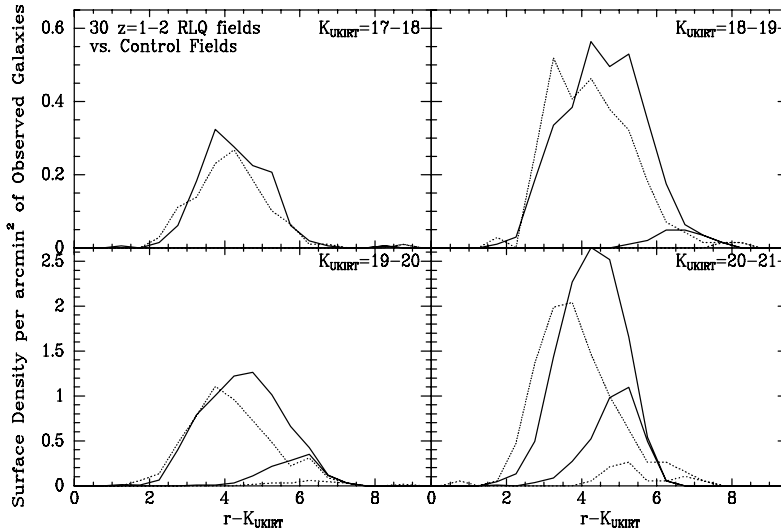


Fig. 11.— Colors of K -selected galaxies. Solid line is $z=1-2$ quasar fields; dotted line is control fields. Smaller histograms represent those galaxies with lower or upper limits to their colors. Each histogram has been normalized by the area imaged in the appropriate magnitude range to yield the surface density of galaxies per arcmin² in each color bin. The K_{UKIRT} magnitude range is given in each panel. The vertical scales differ between the top and bottom panels.

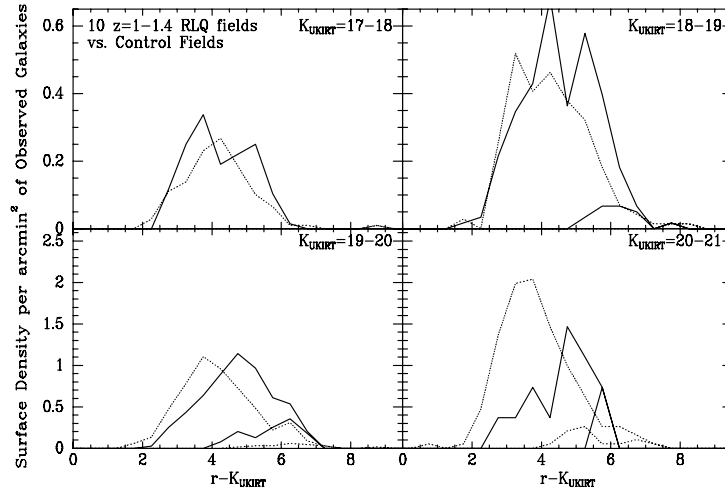


Fig. 12.— Colors of K -selected galaxies. Solid line is $z=1-1.4$ quasar fields; dotted line is control fields. Smaller histograms represent those galaxies with lower or upper limits to their colors. Each histogram has been normalized by the area imaged in the appropriate magnitude range to yield the surface density of galaxies per arcmin² in each color bin. The K_{UKIRT} magnitude range is given in each panel. The vertical scales differ between the top and bottom panels. Only a handful of galaxies in one quasar field contribute to the $K_{UKIRT}=20-21$ magnitude range, so the difference in those two histograms is not significant.

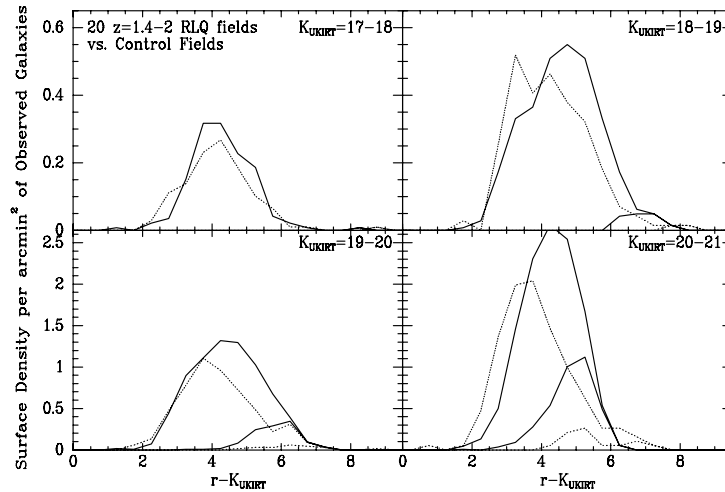


Fig. 13.— Colors of K -selected galaxies. Solid line is $z=1.4-2$ quasar fields; dotted line is control fields. Smaller histograms represent those galaxies with lower or upper limits to their colors. Each histogram has been normalized by the area imaged in the appropriate magnitude range to yield the surface density of galaxies per arcmin² in each color bin. The K_{UKIRT} magnitude range is given in each panel. The vertical scales differ between the top and bottom panels.

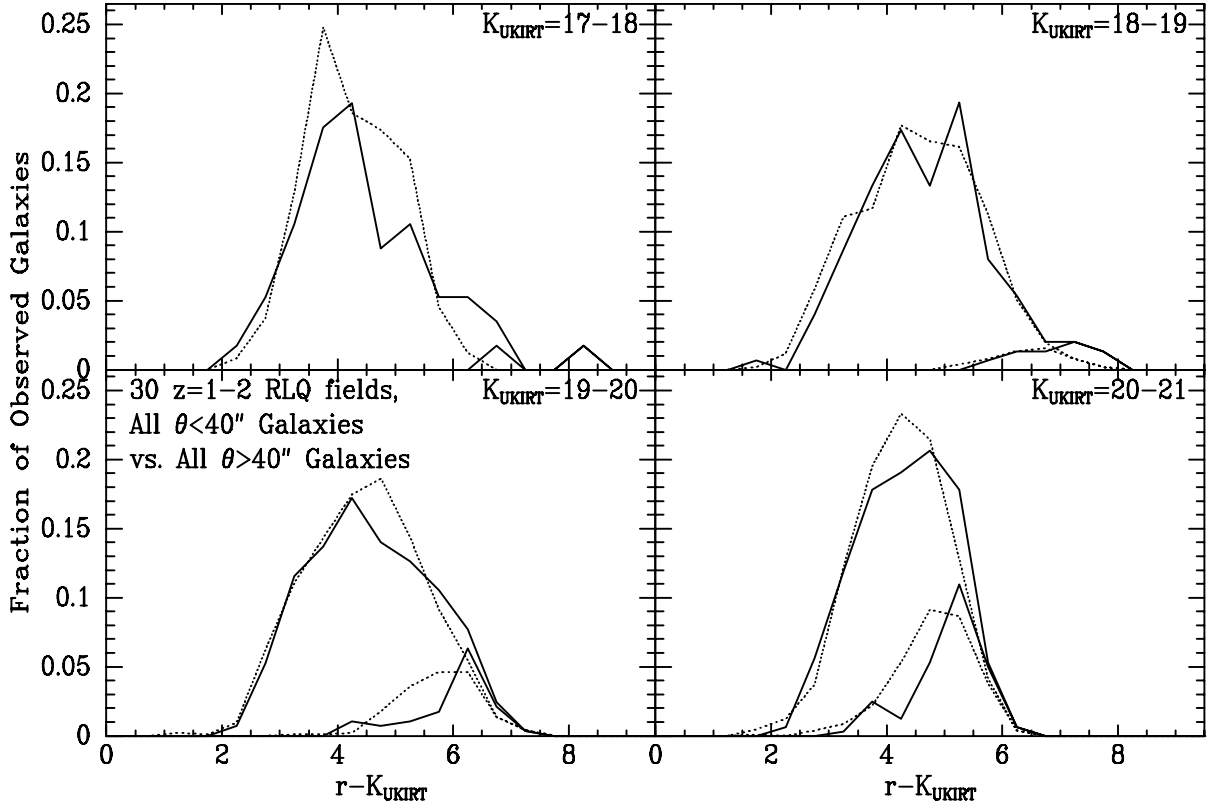


Fig. 14.— Colors of K -selected galaxies in $z=1-2$ RLQ fields. Solid line is galaxies at $\theta < 40''$ from the quasars; dotted line is galaxies at $\theta > 40''$ from the quasars. Smaller histograms represent galaxies with lower or upper limits to their colors. The K_{UKIRT} magnitude range is given in each panel.

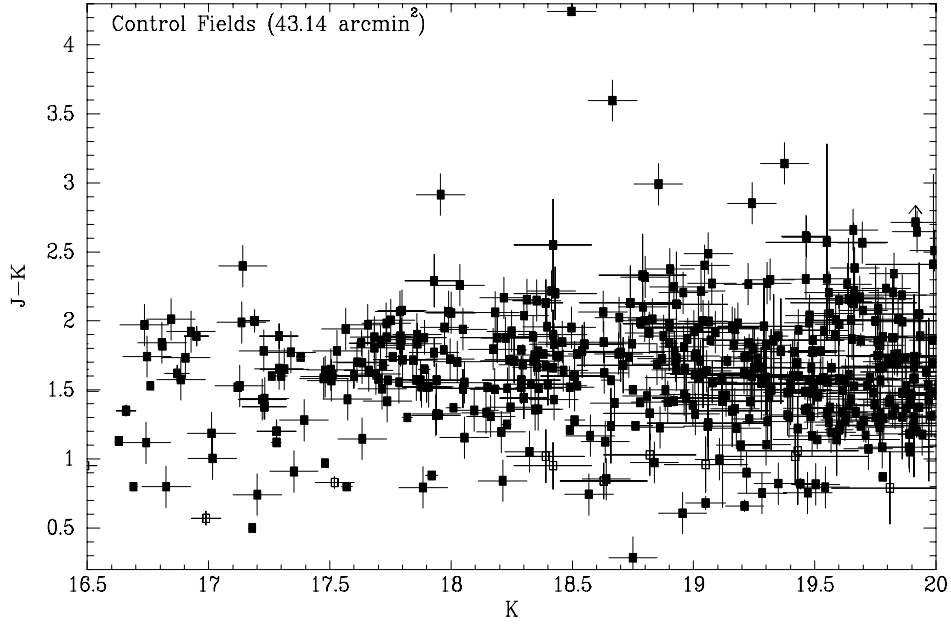


Fig. 15.— $K/J-K$ color-magnitude diagram for galaxies in the control field datasets of McLeod *et al.* (1995), Elston, Eisenhardt, & Stanford (1998), and Dickinson *et al.* (1998). Open symbols are stars and filled symbols are galaxies, but classifications are only available for the McLeod dataset.

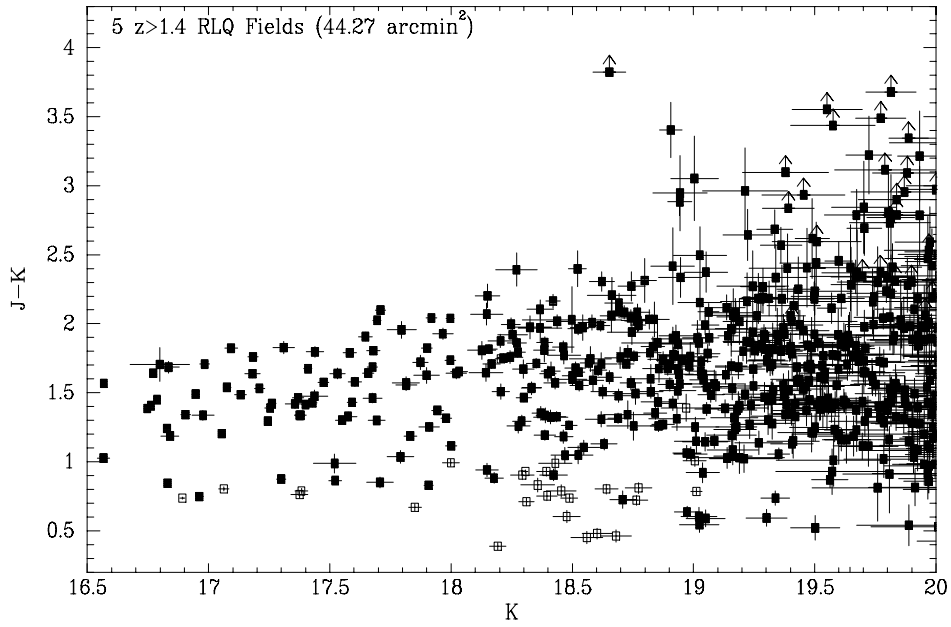


Fig. 16.— $K/J-K$ color-magnitude diagram for galaxies in the five $z=1.4-2$ RLQ fields with J data. Open symbols are stars and filled symbols are galaxies.

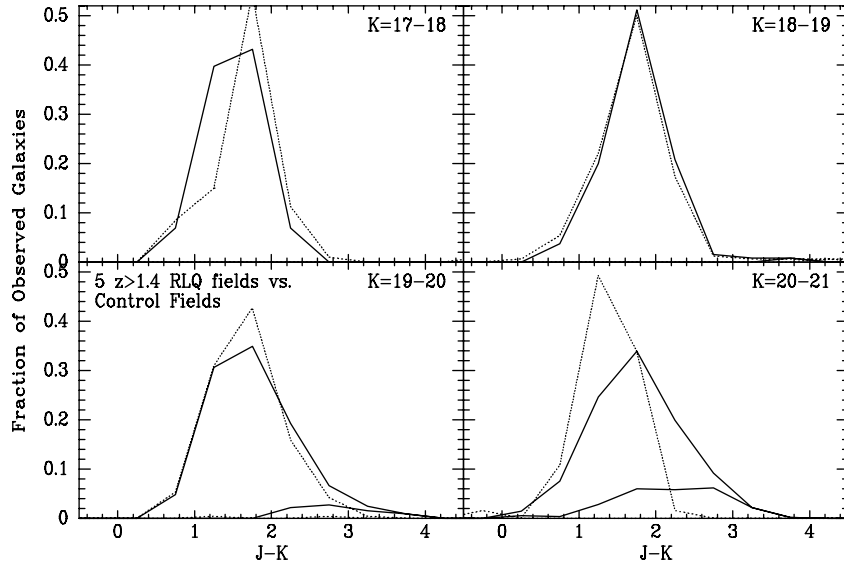


Fig. 17.— $J-K$ colors of K -selected galaxies. Solid line is 5 $z=1.4-2$ RLQ fields with J data; dotted line is control fields. Smaller histograms represent those galaxies with lower or upper limits to their colors. Each histogram has been separated normalized to unity sum. The K_{UKIRT} magnitude range is given in each panel.

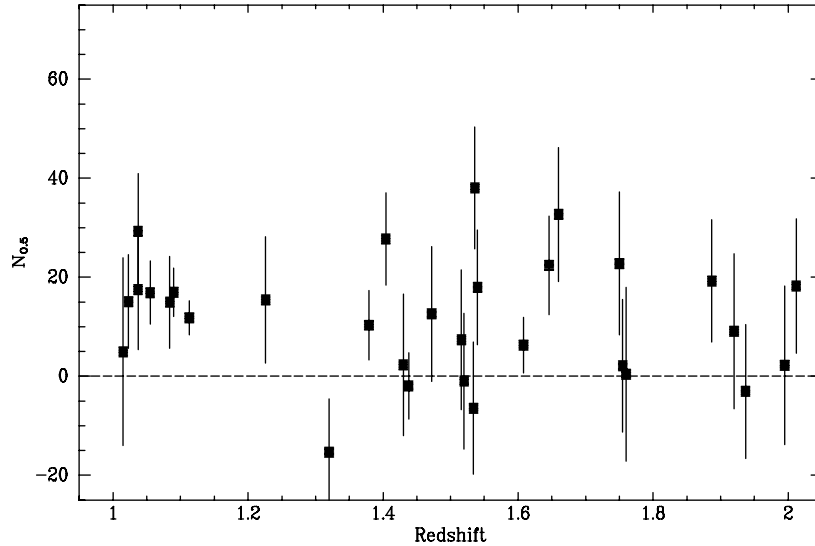


Fig. 18.— The Hill & Lilly (1991) richness statistic $N_{0.5}$ measured in our RLQ fields. Error bars are Poisson only. The horizontal dashed line at $N_{0.5}=0$ shows where the observed counts at <0.5 Mpc equal the prediction from data at >0.5 Mpc.

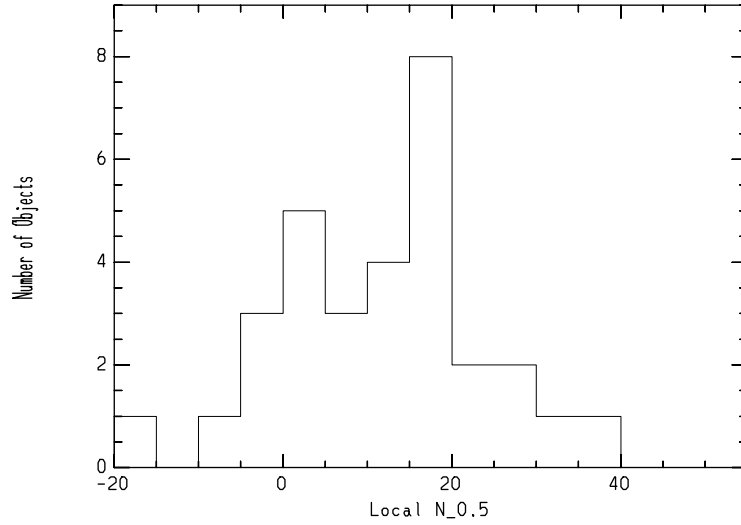


Fig. 19.— Histogram of “near-field” $N_{0.5}$ values measured for our RLQ fields. Abell richnesses of 0, 1, and 2 are approximately $N_{0.5}=10, 19,$ and 31.

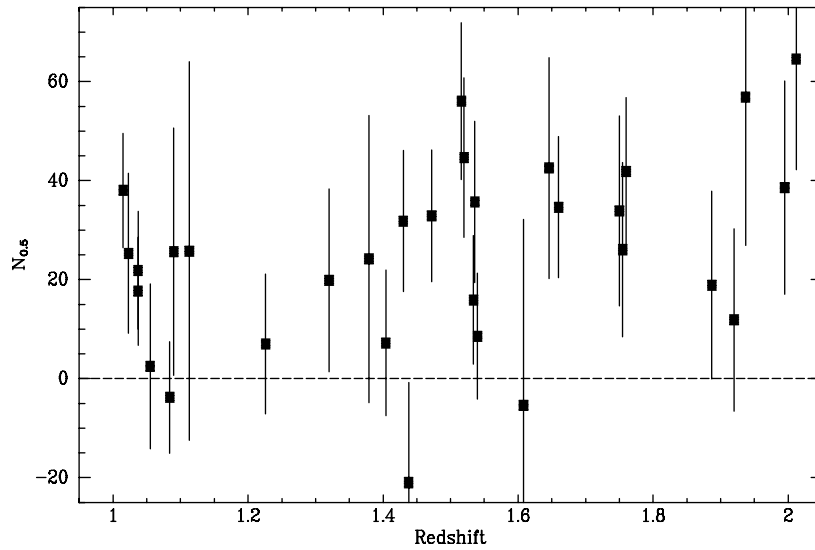


Fig. 20.— The Hill & Lilly (1991) richness statistic $N_{0.5}$ measured for our RLQ fields compared to the literature. Error bars include the uncertainties in the corrections for fields which do not reach $K_{BCG}+3$. The horizontal dashed line at $N_{0.5}=0$ shows where the observed counts at <0.5 Mpc equal the prediction from the average published literature data.

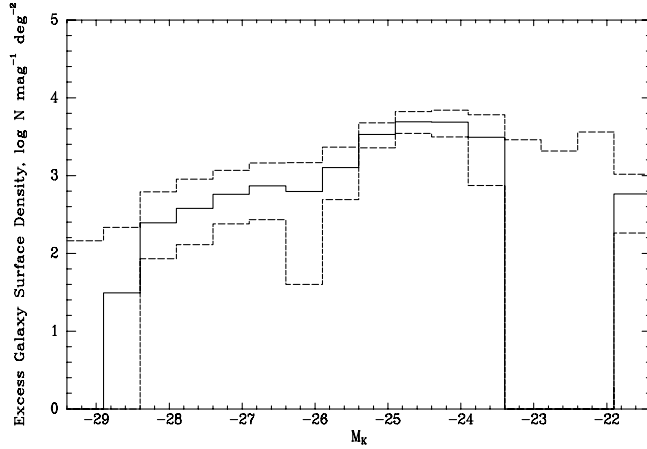


Fig. 21.— The solid line is the excess galaxy surface density ($\log N$) vs. M_K . Dashed lines show the $\pm 1\sigma$ uncertainty envelope. The excesses from all $z < 1.4$ fields have been coadded and normalized by the area at each magnitude bin to make this plot.

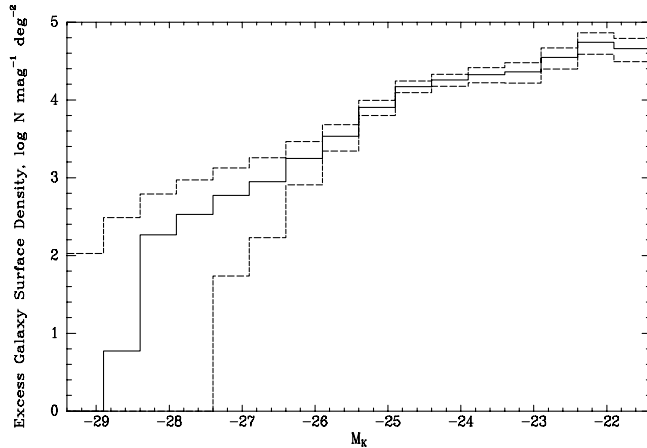


Fig. 22.— The solid line is the excess galaxy surface density ($\log N$) vs. M_K . Dashed lines show the $\pm 1\sigma$ uncertainty envelope. The excesses from all $z > 1.4$ fields have been coadded and normalized by the area at each magnitude bin to make this plot. Even though these fields are at higher redshift, better data enables us to reach farther down the luminosity function in them than in the $z < 1.4$ fields, on average.

Fig. 23.— Color image of the field of Q 0835+580 ($z=1.534$) using rJK_s images to drive the blue, green and red color guns, respectively. Saturation occurs at $r=24$, $K_s=20$, and $J=21$ mag/arcsec². North is up and East is left; the area in black is approximately $3.25'$ by $3.25'$.

Fig. 24.— Color image of the field of Q 1126+101 ($z=1.516$). See key to Figure 23 for details. The area in black is approximately $3.3'$ by $3.3'$.

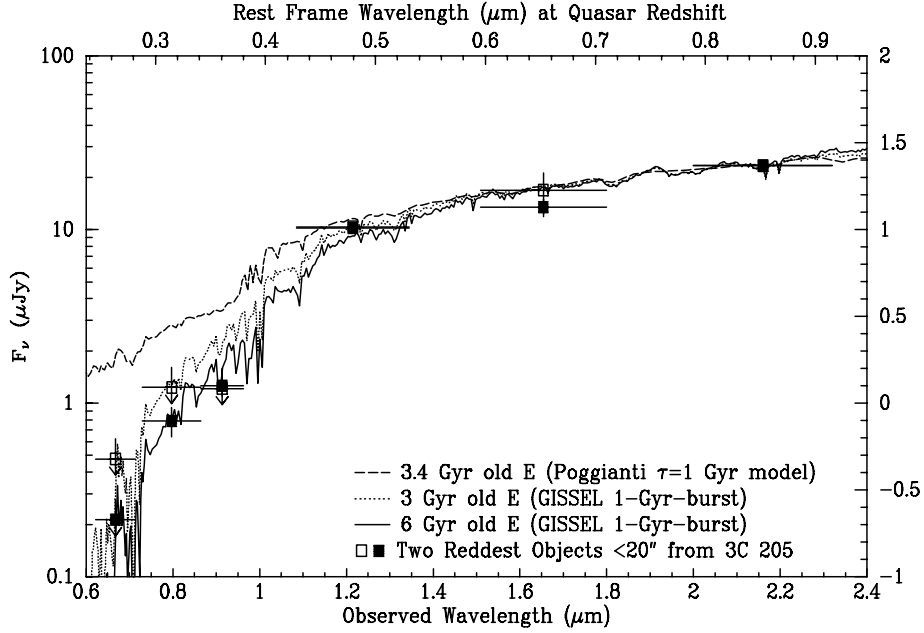


Fig. 25.— The SEDs for the two reddest objects in $r-K_s$ within $\theta=20''.5$ of Q 0835+580 ($z=1.534$) are shown as the filled and open squares with Poisson error bars on the fluxes. Data points are plotted at the effective wavelengths of each filter, and horizontal error bars indicate the widths of the filters. Model spectra are as shown on the figure and discussed in the text.

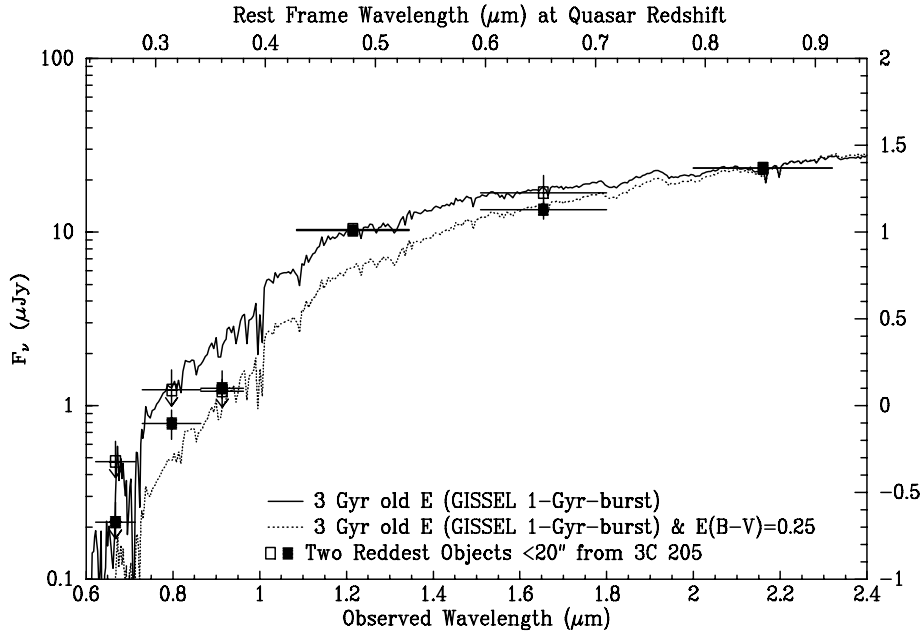


Fig. 26.— See key to Figure 25 for details. Model spectra are as shown on the figure and discussed in the text.

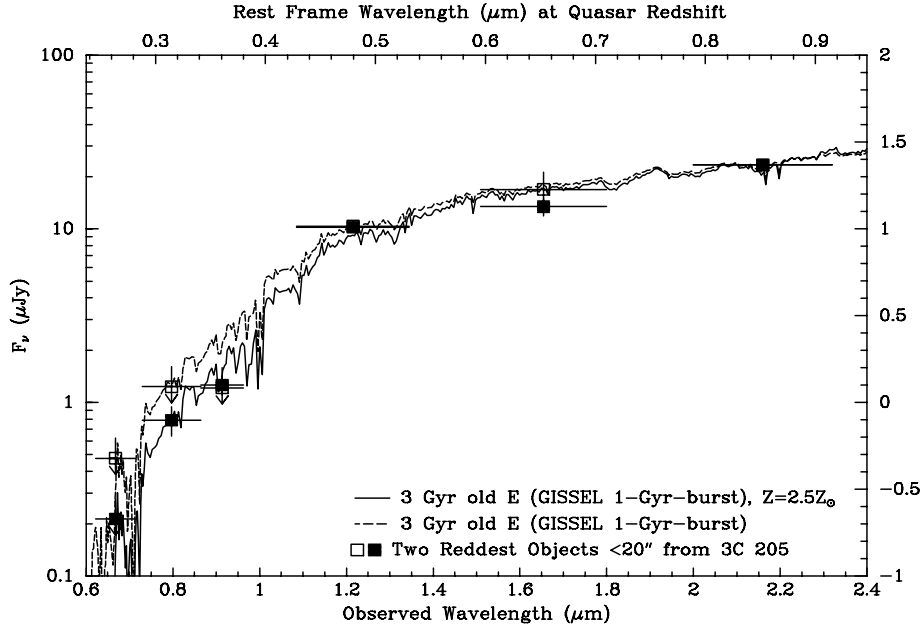


Fig. 27.— See key to Figure 25 for details. Model spectra are as shown on the figure and discussed in the text.

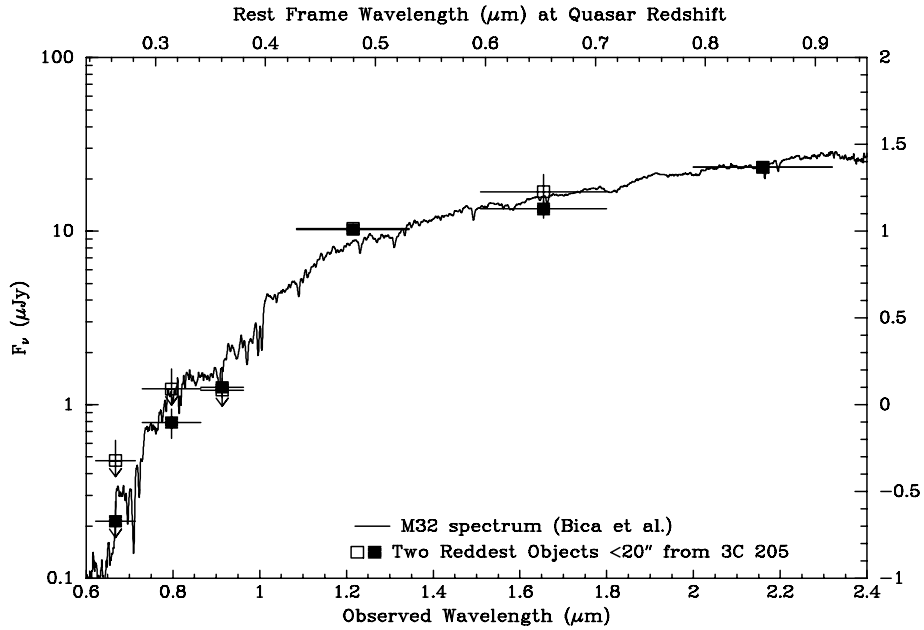


Fig. 28.— The SEDs for the two reddest objects in $r-K_s$ within $\theta=20''.5$ of Q 0835+580 ($z=1.534$) are shown as the filled and open squares with Poisson error bars on the fluxes. Horizontal error bars indicate the widths of the filters used to construct the SEDs. The Bica *et al.* (1996) spectrum of M32 is shown as the solid line.

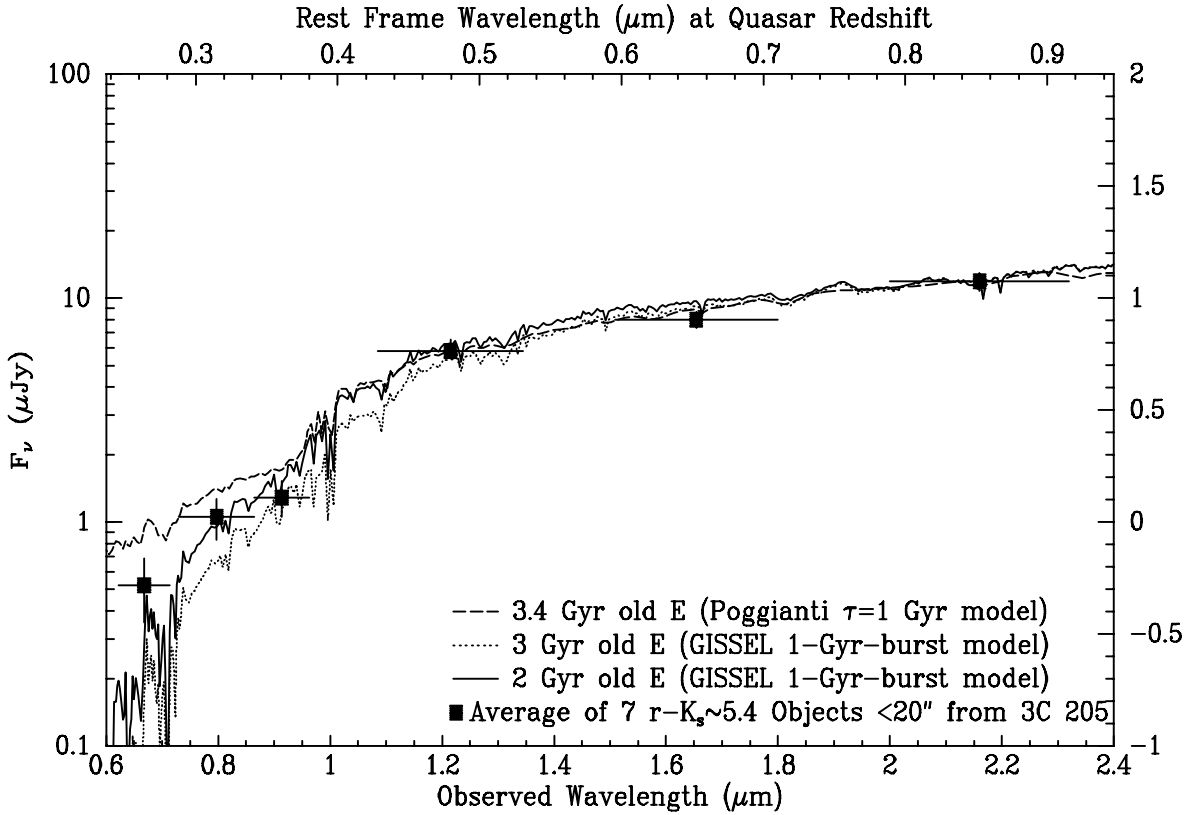


Fig. 29.— The average SED for the seven next reddest objects in $r-K_s$ within $\theta=20''.5$ from Q 0835+580 ($z=1.534$) is shown as the filled squares and Poisson error bars on the fluxes. Horizontal error bars indicate the widths of the filters used to construct the SEDs. Model spectra are as shown on the figure and discussed in the text.

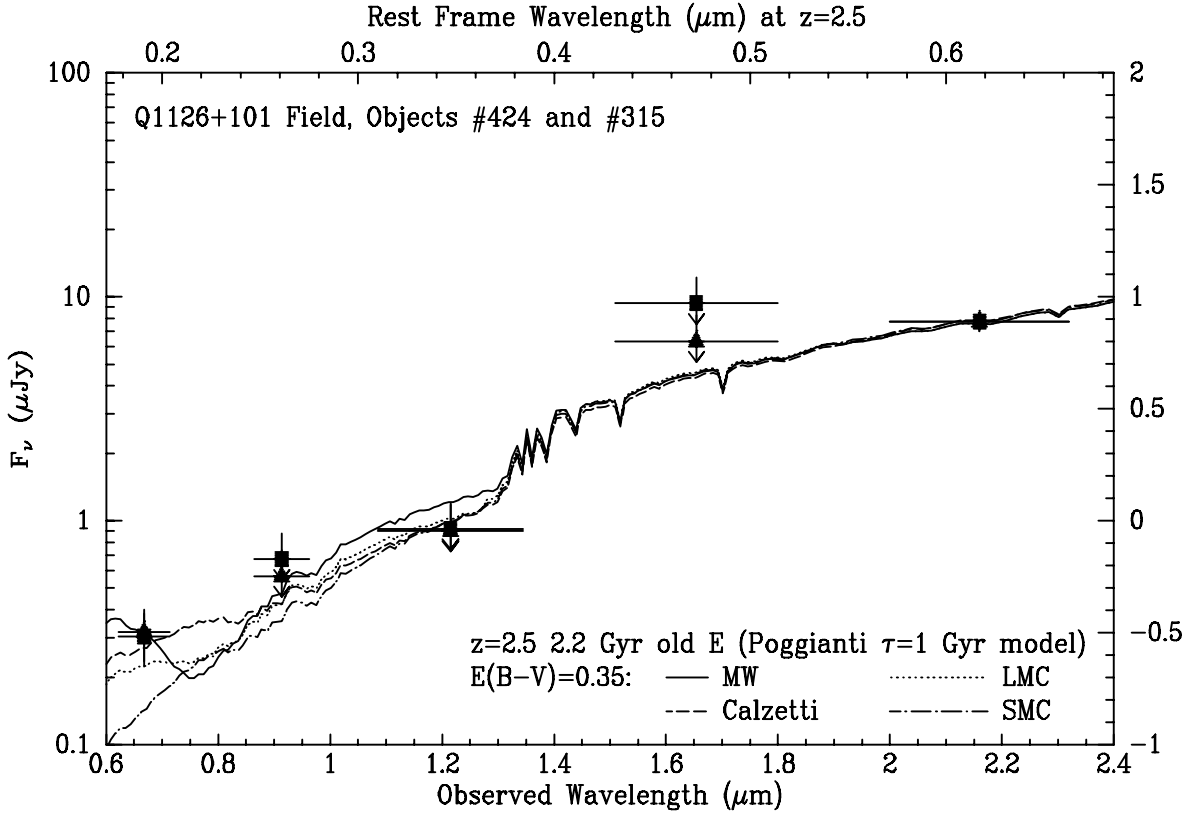


Fig. 30.— The data points are the two objects with $r-K_s > 5$ which are reddest in $J-K_s$ in the Q 1126+101 field, #424 (triangles) and #315 (squares), normalized to the same flux in K_s . The lines are the 2.2 Gyr old E model of Poggianti (1997) reddened by different extinction laws with $E(B-V)=0.35$ and normalized to the data in K_s . Solid line is the Milky Way (MW) extinction law from Seaton (1979) and Howarth (1983). Dashed line is the extinction law from Calzetti (1997). Dotted line is the LMC extinction law from Howarth (1983). Dash-dot line is the SMC extinction law given by a linear (in $1/\lambda$) fit to the data of Prévot *et al.* (1984). All extinction laws have been normalized to $R_V=3$. The relative extinctions for the various laws are significantly different only at rest-frame $\lambda < 3800 \text{ \AA}$.

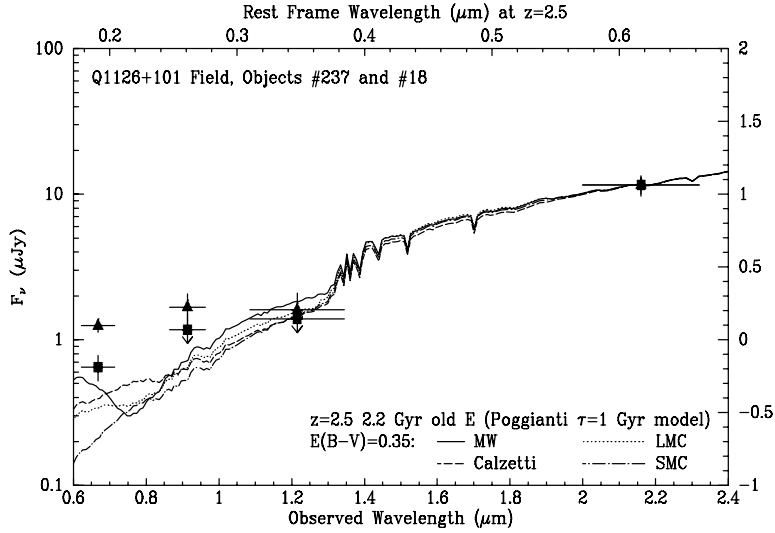


Fig. 31.— The data points are the two objects with $r-K_s < 5$ which are reddest in $J-K_s$ in the Q 1126+101 field, #237 (triangles) and #18 (squares), normalized to the same flux in K_s . The lines are the 2.2 Gyr old E model of Poggianti (1997) reddened by the same extinction laws as in Figure 30, with $E(B-V)=0.35$.

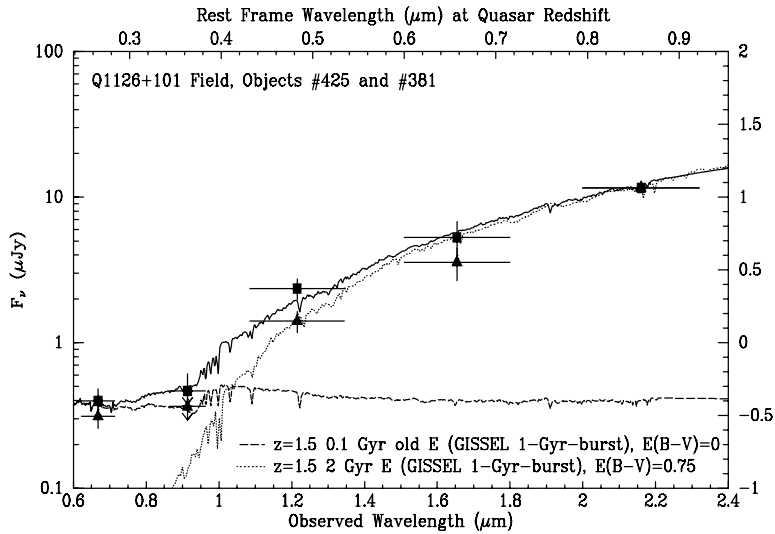


Fig. 32.— The data points are the two objects with $J-K_s > 2.5$ in the Q 1126+101 field which have believable detections in H , #425 (triangles) and #381 (squares), normalized to the same flux in K_s . The dotted line is a 2 Gyr old GISSEL model E reddened by $E(B-V)=0.75$ using the extinction law from Calzetti (1997) and normalized to the data in K_s . The dashed line is a 0.1 Gyr old unreddened GISSEL model E normalized to the data in r . The solid line is the sum of the two.

This figure "rjk0835_scale.gif" is available in "gif" format from:

<http://arxiv.org/ps/astro-ph/9806151v1>

This figure "rjk1126_scale.gif" is available in "gif" format from:

<http://arxiv.org/ps/astro-ph/9806151v1>